Journal of Cleaner Production 272 (2020) 122517

Contents lists available at ScienceDirect

Journal of Cleaner Production

journal homepage: www.elsevier.com/locate/jclepro

Pyrolysis of torrefied biomass: Optimization of process parameters using response surface methodology, characterization, and comparison of properties of pyrolysis oil from raw biomass

Satyansh Singh , Jyoti Prasad Chakraborty *, Monoj Kumar Mondal

Department of Chemical Engineering and Technology, Indian Institute of Technology (Banaras Hindu University), Varanasi, 221005, Uttar Pradesh, India

ARTICLE INFO

Article history:
Received 16 February 2020
Received in revised form
28 May 2020
Accepted 30 May 2020
Available online 1 July 2020

Handling editor: Cecilia Maria Villas Bôas de Almeida

Keywords:
Acacia nilotica
Torrefied biomass
Pyrolysis
Optimization
Response surface methodology

ABSTRACT

Pyrolysis of torrefied *Acacia nilotica* was investigated in a tubular fixed-bed reactor under nitrogen environment. The process was optimized using response surface methodology coupled with central composite design, in order to obtain the maximum yield of pyrolysis oil. The maximum yield of pyrolysis oil (33.59 wt %) was obtained at 507.04 °*C*, retention time of 58.25 min, heating rate of 38.00 °*C*/min, and sweeping gas flow rate of 40.52 mL/min. Analysis of variance confirmed that pyrolysis of torrefied biomass for maximum pyrolysis oil yield highly depended on temperature followed by heating rate, retention time, and sweeping gas flow rate, respectively. Pyrolysis of raw biomass was also carried out at the optimum condition for comparing the quality of both pyrolysis oils. The pyrolysis oil samples were subjected to FTIR, GC-MS, and ^{13}C NMR analyses along with estimation of water content, pH, viscosity, HHV, etc., for comparing the physicochemical characteristics. Results showed that total aromatic carbon, carbonyl carbon, and primary alkyl carbon of pyrolysis oil from torrefied biomass increased by 40.28, 51.36, and 6.34%, respectively, as compared to pyrolysis oil from raw biomass. The phenol derivative compounds are increased by 18.91%. The HHV and pH of pyrolysis oil from torrefied biomass increased by 23.53, 42.15%, respectively, while water content decreased by 34.37% as compared to pyrolysis oil from raw biomass. Thus, with rapid advancement in pyrolysis process, the integrated approach of torrefaction-pyrolysis process may be beneficial to produce cleaner pyrolysis oil as compare to raw biomass.

1. Introduction

Fossil-derived fuels such as crude petroleum, coal, and natural gas continue to provide most of the energy for different sectors such as industrial, transportation, and day to day utilization (Sakthivel et al., 2019). As per the International Energy outlook 2016, fossil fuels will continue to supply 78% of the total energy requirement of the world till 2040 (Mohammed et al., 2017b). The fossil fuel reserves are neither sustainable nor clean sources of energy. Also, the majority of fossil fuel reserves are found in a specific geographical location of the world (Korshunov et al., 2019). Anthropogenic extraction of energy from fossil fuels has detrimental environmental impacts, for example, global warming and emission of greenhouse gases (Dhyani and Bhaskar, 2018). Also, due to the fast-growing population, technological advancement and higher standard of living of people, demand for energy as well as the price of fossil-derived fuels like petrol and diesel are increasing (Kadlimatti et al., 2019).

So, to mitigate these challenges, the world's renowned agencies (International Energy Agency (IEA), United Nations Framework Convention on Climate Change (UNFCCC)) and the government of various nations have taken significant steps. The United Nations climate change conference (November 2015) has fixed a goal for limiting the global temperature upsurge to below 2 °*C* (Mohammed et al., 2017b). As per the national bio-fuel policy, India has targeted the blending of 25% bio-fuels with fossil-derived fuel by 2030 (Sakthivel et al., 2020). A major thrust is given to renewable sources like biomass, solar, wind, hydrothermal, and geothermal for extraction of energy (Sakthivel et al., 2019). Among the available renewable sources of energy, incidentally, biomass has gathered significant attention by different research societies of the world due to its copious amount, low market value, and carbon neutrality due to its inherent CO_2 cycle (Dhyani and Bhaskar, 2018).

Acacia nilotica is a tropical forest tree and widely available in

* Corresponding author.
E-mail address: jpc.che@iitbhu.ac.in (J.P. Chakraborty).

https://doi.org/10.1016/j.jclepro.2020.122517
0959-6526/

Nomenclature

Abbreviations

ANOVA	Analysis of variance
ASTM	American Society for testing and materials
PO-RAW	Pyrolysis oil from raw biomass pyrolysis at optimum condition
PO-TB	Pyrolysis oil from torrefied biomass pyrolysis at optimum condition
CCD	Central composite design
CHNS	Carbon Hydrogen Nitrogen Sulfur
FTIR	Fourier transformed infrared spectroscopy
FC	Fixed carbon (wt %)
GC-MS	Gas chromatography-mass spectroscopy
HHV	Higher heating value (MJ/kg)
HR	Heating rate ($^{\circ}C$ /min)
MC	Moisture content (wt %)
RSM	Response surface methodology
RT	Retention time (min)
SGF	Sweeping gas flow rate (mL/min)
T	Temperature ($^{\circ}C$)
TB	Torrefied biomass

many countries of Asian, African, and Australian continents. The height and diameter of *Acacia nilotica* vary between 7 and 18 m and 20–30 cm, respectively (Singh et al., 2020a). These trees are rapidly growing, typically located in low-productivity waste and sterile land. Also, they do not contend with land for agriculture and other applications. It has also been recognized as a valuable tree of economic value because of its medicinal use and source of gums and tannins (Saratale et al., 2019). *Acacia nilotica* also provides forest wood and fodder for animals in countryside areas of India. In India, 167 tons of wood are produced per hectare of land, while 0.6 million tons of pods get generated every year from *Acacia nilotica* (Singh et al., 2019, 2020b). It has also been considered as excellent fuelwood because of higher heating value (~20 MJ/kg) and its tendency to produce less smoke while burning (Singh et al., 2020b). It is widely used in brick kiln, textile, and paper industries as a fuel for boilers (Singh et al., 2020b).

In this regard, thermochemical processes, for example, combustion, pyrolysis, torrefaction, and gasification, have gained attraction to convert biomass into biofuels due to higher yield of product, lower operational cost, speed of reaction and higher efficiency (Dhanavath et al., 2019). In particular, pyrolysis has gained dominance for conversion of biomass into biochar, pyrolysis oil, and valuable gases (Abas et al., 2018). In pyrolysis process, biomass gets decomposed at elevated temperature in an inert atmosphere (Dai et al., 2019). Pyrolysis oil has been considered as most valuable product from pyrolysis (Guedes et al., 2018). The pyrolysis process is driven by many factors, for example, process temperature (T), retention time (RT), heating rate (HR), sweeping gas flow rate (SGF), and particle size, etc. (Dhyani and Bhaskar, 2018). The optimization of these process parameters becomes very important when it comes to efficiency, economy, and scale-up of pyrolysis reactor system (Singh et al., 2019). The optimization of process parameters by varying one parameter keeping others constant, e.g., one factor at a time (OFAT) method, does not holistically consider the complex nature of pyrolysis process, and it consumes a lot of time to complete multiple experiments to obtain the optimum value (Singh et al., 2019). Also, the interaction between different process parameters cannot be understood by the above method. The response surface methodology (RSM) is a statistical tool that may be employed to optimize the process parameters by considering all the parameters simultaneously (Singh et al., 2019). The RSM with the central composite design (CCD) technique has already been implemented by many researchers to optimize the process and to examine the individual and interaction effect of different parameters, while performing lesser number of experimental runs.

The pyrolysis oil is an intense dark brown-colored liquid that consists of a large number of chemical compounds (Dhyani and Bhaskar, 2018). Currently, pyrolysis oil is receiving enormous interest since it is regarded as a second-generation biofuel (Lazzari et al., 2019) and may be utilized as a fuel in furnaces, boilers, and engines for generation of heat and power (Zhang et al., 2017) or it may be a good source of various chemicals (Dhyani and Bhaskar, 2018). The pyrolysis of different types of raw biomass and optimization of process parameters for maximum yield of pyrolysis oil has been investigated by many researchers, as mentioned in Table 1. However, pyrolysis oil obtained from raw biomass has some drawbacks, for example, high water content, poor volatility, higher acidic value, low heating value, chemical instability, and undesired aging problem (Ro et al., 2018; Zhang et al., 2017). These characteristics of pyrolysis oil hampered its direct and efficient utilization as fuel (Zhang et al., 2017). Thus, it cannot compete with conventional fuels such as gasoline and diesel. So, there is an urgent demand for upgrading of pyrolysis oil. Various efforts have been made in this field such as catalytic pyrolysis and pretreatment of biomass by torrefaction (Singh et al., 2019), hydrothermal liquefaction (Nazari et al., 2017) prior to pyrolysis.

Among various pretreatment processes, torrefaction is considered as one of the most promising and economical processes (Dai et al., 2019). Torrefaction can enhance the quality of raw biomass by increasing its fixed carbon and higher heating value (HHV) as well as by decreasing its moisture and oxygen content (Singh et al., 2020a). The impact of torrefaction on the quality and quantity of pyrolysis oil is available in published literature (Chen et al., 2015a; Gogoi et al., 2017; Xin et al., 2018). Table 2 represents the pyrolysis of various torrefied biomass (TB) and effect of torrefaction on the quality of pyrolysis oil. In most of the studies, torrefaction was performed from 200 to 300 $^{\circ}C$ with retention time less than or equal to 60 min. The desired output has been solid yield of TB. Afterward, pyrolysis of TB was carried out to obtain high-quality pyrolysis oil.

The base of the torrefaction is to optimize the operating condition, which can yield improved quality TB. However, pyrolysis of that improved TB (having maximum HHV and energy yield simultaneously) gained at optimum condition of torrefaction has not been investigated. Less attention has been given towards HHV and energy yield of TB. The HHV and energy yield of TB are very crucial parameters for energy utilization and densification (Singh et al., 2019) and play a vital role in deciding quality and quantity of pyrolysis oil obtained from pyrolysis of TB. Both these parameters display opposite trend during torrefaction process. The HHV of TB increased, while energy yield decreased with temperature. Thus, considering these two parameters, torrefaction process has to be optimized for maximum HHV and energy yield of TB. In our previous work, we have optimized the torrefaction process for maximum HHV and energy yield (Singh et al., 2019). The optimum condition was attained at 252 $^{\circ}C$, retention time of 60 min, and heating rate of 5 $^{\circ}C$/min.

Therefore, in this work, two-stage optimization (optimization of torrefaction process (Stage-1), optimization of pyrolysis process (Stage-2)) of integrated torrefaction-pyrolysis process has been reported. The pyrolysis of TB obtained at optimum condition was examined in a tubular quartz reactor. The independent process parameters such as temperature, RT, HR, and SGF were optimized

Table 1
Pyrolysis of different raw biomass and optimization of process parameters using response surface methodology.

Biomass	Desired outcomes	Optimum condition	Optimization tool	References
Pyrolysis of various raw biomass				
Napier grass	Bio-oil yield (50.57 wt %)	T: 600 °C, HR; 50 °C/min, SGF: 5 L/min	RSM based CCD	Mohammed et al. (2017b)
Oil Palm Fiber	Bio-oil yield (50.57 wt %)	T: 536.5 °C, RT: 23.88 min, AC loading: 86.21 g	RSM based CCD	Abas et al. (2018)
Bambara groundnut	Bio-oil yield (36.49 wt %)	T: 600 °C, HR: 50 °C/min, SGF: 11 L/min	RSM based CCD	Mohammed et al. (2017a)
Sagwan sawdust	Bio-oil yield (48.70 wt %)	T: 640 °C, SGF: 180 mL/min, Bed height: 8 cm	RSM based BBD	Gupta and Mondal (2019)
Food waste	Bio-oil yield (30.24 wt %)	T: 400 °C, RT: 30 min, SGF: 50 mL/min	RSM based CCD	Kadlimatti et al. (2019)
Perennial grass	Bio-oil yield (38.1 wt %)	T: 550 °C, HR: 20 °C/min, SGF: 226 mL/min	RSM based CCD	Saikia et al. (2018)
Neem press seed cake	Bio-oil yield (52.1 wt %)	T: 512.5 °C, RT: 60 min, SGF: 0.5 L/min	RSM based BBD	Dhanavath et al. (2019)
Pine needles	Bio-oil yield (27.6 wt %)	T: 547 °C, HR: 50 °C/min, VCT: 15 °C, SGF: 1.85 L/min	RSM based CCD	Mandal et al. (2018)
Euphorbia rigida	Bio-oil yield (35.3 wt %)	T: 600 °C, HR: 200 °C/min, SGF: 100 mL/min	RSM based CCD	Kılıç et al. (2014)
Torrefied *Acacia nilotica*	Pyrolysis oil yield (33.59 wt %)	T: 507.04 °C, HR: 38 °C/min, RT: 58.25 min, SGF: 40.52 mL/min	RSM based CCD	**Present Work**

T, Temperature; HR, Heating rate; RT, Retention time; SGF, Sweeping gas flow rate; VCT, vapor cooling temperature; RSM, response surface methodology; CCD, central composite design; BBD, Box-Behnken design technique.

Table 2
Pyrolysis of different TB.

Biomass	Torrefaction condition	Pyrolysis condition	Important findings[a]	References
Pyrolysis of TB				
Arecanut husk	T; 200–300 °C, HR; 10 °C/min, RT; 30 min	T; 300–600 °C, HR; 40 °C/min	The bio-oil yield decreased from 32 to 21%, O/C ratio of bio-oil decreased from 0.36 to 0.28	Gogoi et al. (2017)
Loblolly pine	T; 273–330 °C, RT; 2.5 min	T; 500 °C, FR; 150 g/h	O/C ratio of bio-oil decreased from 0.63 to 0.31, while, HHV of bio-oil increased from 20 to 26.3 MJ/kg	Meng et al. (2012)
Cotton stalk	T; 220–280 °C, RT; 30 min	T; 500 °C	Acid and furan content of bio-oil decreased, while, phenolic and ketone derivatives increased from 0.53 to 8.25, 0.59–6.41%, respectively.	(Chen et al., 2015a)
Rice straw	T; 225–275 °C, RT; 30 min	T; 450–500 °C, HR; 1000 °C/sec	Oxygenated, acid, aldehydes, ketones, and sugar derivative compounds, as well as water content of bio-oil, decreased	Zheng et al. (2012)
Yunnan pine	T; 210–300 °C, RT; 30 min	T; 500 °C	The bio-oil yield decreased from 37 to 20%, phenolic and hydrocarbon derivatives increased, while, acid, aldehydes and ketone derivative compounds decreased	Zheng et al. (2017)
Rice straw	T; 240 °C, RT; 60 min	T; 550 °C	Phenolic compounds increased from 28 to 42%, while, acid, aldehydes, ketone and furan derivative compounds decreased	Dong et al. (2018)
Corncob	T; 210–300 °C, RT; 20–60 min	T; 600 °C, HR; 20000 K/s (catalytic pyrolysis)	The yield of bio-oil increased to 82% from 51%, aromatic compounds increased	Zheng et al. (2014)
Corn stalk	T; 200–290 °C, RT; 30 min	T; 550 °C	Bio-oil yield decreased as compared to raw biomass	Wang et al. (2018)
Herbaceous residue	T; 210–280 °C, RT; 60 min	T; 600 °C, HR; 50 °C/min	Phenol, acid, ketone, ester and furan derivative compounds are the main components of bio-oil and collectively contribute 72.1% of total compounds detected.	Xin et al. (2018)

[a] Important findings are mentioned with respect to the pyrolysis of raw biomass at similar pyrolysis conditions; T, Temperature; HR, Heating rate; RT, Retention time; FR, feed rate.

for the highest yield of pyrolysis oil using RSM based CCD technique. The physicochemical properties of pyrolysis oil obtained at optimum condition of pyrolysis of raw and TB were compared for water content, HHV, pH, ash content, carbon residue, FTIR, GC-MS, and ^{13}C NMR analyses. Further, the characteristics of biochar and pyrolytic gaseous obtained from pyrolysis of raw and TB at optimum conditions were also characterized.

2. Experimental segment

2.1. Sample preparation

Torrefied *Acacia nilotica* at optimum torrefaction condition of 252 °C, 60 min of RT, and 5 °C/min of HR obtained in our previous work (Singh et al., 2019) were used for conducting experimental runs on pyrolysis. Multiple runs were performed at optimum torrefaction condition for collection of TB. The detailed discussion about collection and preparation of raw biomass may be obtained from Singh et al. (2019). The proximate, ultimate analyses, and HHV of raw biomass and TB at optimum condition are given in Table 3.

2.2. Design of experimental condition using RSM

To increase the pyrolysis oil yield, it is imperative to know the behavior of each parameter towards the pyrolysis process. This can be done by optimization of process parameters affecting the pyrolysis process. RSM has been considered as one of the most promising and prevalent techniques used for the optimization of process. A three-level, four-factor CCD technique was employed to optimize the independent process variables. The CCD technique was used since it requires minimum set of experimental runs to establish a correlation among independent variables and desired

Table 3
Characteristics of raw and TB obtained at optimum condition of torrefaction.

Characteristics	Raw biomass[a]	TB252-60-5[b]
Moisture content (wt. %)	6.24	1.67
Ash content (wt. %)	0.65	1.42
Volatile matter (wt. %)	80.36	44.78
Fixed carbon (wt. %)	12.75	52.13
C (wt. %)	44.24	59.52
H (wt. %)	7.52	4.76
O (wt. %)	48.23	35.52
N (wt. %)	BDL	BDL
S (wt. %)	BDL	BDL
H/C	0.17	0.08
O/C	1.09	0.60
Higher heating value (MJ/kg)	19.31	23.73

BDL; Below detection limit.
[a] Properties of raw biomass were taken from Singh et al. (2019).
[b] TB obtained at optimum condition of 252 °C, 60 min RT, and 5 °C/min HR in our previous study Singh et al. (2019).

response. Temperature (A), RT (B), HR (C) and SGF (D) in the range of 400–600 °C, 30–90 min, 15–40 °C/min and 40–80 mL/min, respectively, were considered as independent process parameters and pyrolysis oil yield was considered as the desired response that needs to be maximized. Table 4 represents the coded values of independent process variables. CCD technique consists of axial points (2k), factorial points (2^k), and replicates center points (n_k). The number of experimental runs to be carried out was calculated according to Eq. (1):

$$N = 2^k + 2k + n_k = 2^4 + 2(4) + 6 = 30 \quad (1)$$

where N signifies number of experimental runs to be carried out, k signifies selected independent variables, and n_k signifies number of replicate central points.

The matrix for different experimental conditions is presented in Table 5. As per the design matrix, total of 30 experiments were carried out. The yield of pyrolysis oil as the response were correlated with selected independent variables. Few fundamental steps have to be followed during optimization of process variables. First one is to develop a general mathematical relationship among process response and independent variables, given as:

$$Y = f(X_1, X_2, X_3, \ldots \ldots \ldots, X_n) \quad (2)$$

where Y signifies the desired predicted response, f signifies the mathematical relation between desired predicted response and independent process variables, and $X_1, X_2, X_3, \ldots \ldots . X_n$ signifies n number of independent process variables affecting the desired predicted outcome.

The second step is related to finding the coefficients of developed mathematical co-relation. In CCD technique, usually, a quadratic polynomial equation is suggested for predicting the response. The general quadratic polynomial model of the response can be presented as follows:

Table 4
Coded levels of experimental variables used in CCD method.

Independent process variable	Coded experimental levels		
	− 1	0	+ 1
Temperature (°C): A	400	500	600
Retention time (min): B	30	60	90
Heating rate (°C/min): C	15	27.5	40
Sweeping gas flow rate (mL/min): D	40	60	80

$$Y = \beta_0 + \sum_{i=1}^{k} \beta_i X_i + \sum_{i=1}^{k} \beta_{ii} X_i^2 + \sum_{i_{i>j}}^{k} \sum_{j}^{k} \beta_{ij} X_i X_j \quad (3)$$

where Y signifies the predicted value of the response, β_0, β_i, β_{ii} , and β_{ij} are constant term and coefficient for linear, quadratic, and interaction terms, respectively, in developed model equation. k signifies the number of independent process variables chosen for optimization of process (here k = 4).

In third step, ANOVA is employed to analyze the result of optimization process. The yield of pyrolysis oil, obtained from experiments was taken as actual values, while, predicted values were obtained from a software package (Stat-Ease Design-Expert version 11, USA). The statistical fitness of developed model was investigated by several variables provided in ANOVA analysis. The dependence of yield of pyrolysis oil on different independent variables was checked by p and F values. In addition, various determination coefficients such as R^2, R^2_{pred}, and R^2_{adj}, as well as degree of freedom, were also analyzed to authenticate the reliability of the developed model. Further, the impact of individual and interaction terms of independent process variables on pyrolysis oil yield was examined by 3D surface and contour plots.

2.3. Experimental process for pyrolysis

Fig. 1 displays the experimental setup. A detailed explanation of experimental procedure and set-up may be seen elsewhere (Singh et al., 2019). In this study, similar procedure was followed during pyrolysis. TB was collected by performing several runs at optimum condition of torrefaction obtained in our earlier research work (Singh et al., 2019). The pyrolysis of TB was carried out between 400 and 600 °C with RT 30–90 min, HR 15–40 °C/min, and SGF 40–80 mL/min as per the experimental design matrix presented in Table 5. During each pyrolysis experiment, 4 g of TB was used. Every experiment under similar operating conditions was repeated twice for validation of results. The yield of pyrolysis oil was obtained by using Eq. (4):

$$\text{Pyrolysis oil yield (wt \%)} = \frac{\text{Wt. of bio} - \text{oil(g)}}{\text{Wt. of torrefied biomass (g)}} \times 100 \quad (4)$$

$$\text{Biochar yield (wt \%)} = \frac{\text{Wt. of biochar(g)}}{\text{Wt. of torrefied biomass (g)}} \times 100 \quad (5)$$

$$\text{Pyrolysis gas yield (wt \%)} = 100 - (\text{Pyrolysis oil yield} + \text{Biochar yield}) \quad (6)$$

Now, considering upgraded pyrolysis oil as desired product from pyrolysis of TB, the energy yield and energy conversion efficiency can be obtained by using Eq. (7) and Eq. (8), respectively.

$$\text{Energy yield of pyrolysis oil} = \text{mass yield} \times \frac{HHV\ of\ pyrolysis\ oil}{HHV\ raw\ Acacia\ nilotica} \quad (7)$$

$$\text{Energy conversion efficiency} = \frac{Energy\ output}{Energy\ input} \times 100 \quad (8)$$

where energy input and energy output can be calculated by using Eq. (9) and Eq. (10), respectively.

Table 5
Experimental design matrix, actual and predicted value of responses.

Run	Temp (°C)	Retention time (min)	Heating rate (°C/min)	Sweeping gas flow rate (mL/min)	Pyrolysis oil yield (wt %)	
					Actual	Predicted
1	500 (0)[a]	60 (0)	27.5 (0)	80 (+ 1)	33.46	32.91
2	500 (0)	60 (0)	27.5 (0)	60 (0)	31.65	31.63
3	600 (+ 1)	90 (+ 1)	40 (+ 1)	80 (+ 1)	26.38	26.55
4	600 (+ 1)	30 (− 1)	15 (− 1)	40 (− 1)	23.76	24.23
5	500 (0)	90 (+ 1)	27.5 (0)	60 (0)	28.35	28.70
6	400 (− 1)	90 (+ 1)	15 (− 1)	80 (+ 1)	21.93	21.95
7	600 (+ 1)	90 (+ 1)	15 (− 1)	80 (+ 1)	22.97	22.86
8	400 (− 1)	30 (− 1)	40 (+ 1)	40 (− 1)	22.67	23.22
9	500 (0)	60 (0)	27.5 (0)	60 (0)	31.77	31.63
10	400 (− 1)	90 (+ 1)	40 (+ 1)	40 (− 1)	23.60	23.73
11	500 (0)	60 (0)	27.5 (0)	60 (0)	30.93	31.63
12	600 (+ 1)	30 (− 1)	40 (+ 1)	80 (+ 1)	25.92	26.56
13	400 (− 1)	90 (+ 1)	15 (− 1)	40 (− 1)	21.67	21.48
14	400 (− 1)	30 (− 1)	15 (− 1)	40 (− 1)	23.95	23.37
15	500 (0)	60 (0)	27.5 (0)	60 (0)	31.92	31.63
16	500 (0)	60 (0)	27.5 (0)	60 (0)	31.67	31.63
17	500 (0)	60 (0)	27.5 (0)	60 (0)	31.41	31.63
18	500 (0)	60 (0)	15 (− 1)	60 (0)	30.35	30.98
19	600 (+ 1)	90 (+ 1)	40 (+ 1)	40 (− 1)	26.10	25.99
20	500 (0)	60 (0)	40 (+ 1)	60 (0)	33.51	32.75
21	500 (0)	30 (− 1)	27.5 (0)	60 (0)	30.14	29.65
22	400 (− 1)	60 (0)	27.5 (0)	60 (0)	24.37	24.08
23	600 (+ 1)	30 (− 1)	15 (− 1)	80 (+ 1)	25.81	25.27
24	500 (0)	60 (0)	27.5 (0)	40 (− 1)	32.11	32.51
25	400 (− 1)	30 (− 1)	15 (− 1)	80 (+ 1)	23.06	23.61
26	600 (+ 1)	90 (+ 1)	15 (− 1)	40 (− 1)	21.85	21.60
27	600 (+ 1)	30 (− 1)	40 (+ 1)	40 (− 1)	26.66	26.23
28	600 (+ 1)	60 (0)	27.5 (0)	60 (0)	25.88	26.04
29	400 (− 1)	30 (− 1)	40 (+ 1)	80 (+ 1)	22.91	22.75
30	400 (− 1)	90 (+ 1)	40 (+ 1)	80 (+ 1)	23.52	23.49

[a] Values in the parenthesis are coded level in response surface methodology.

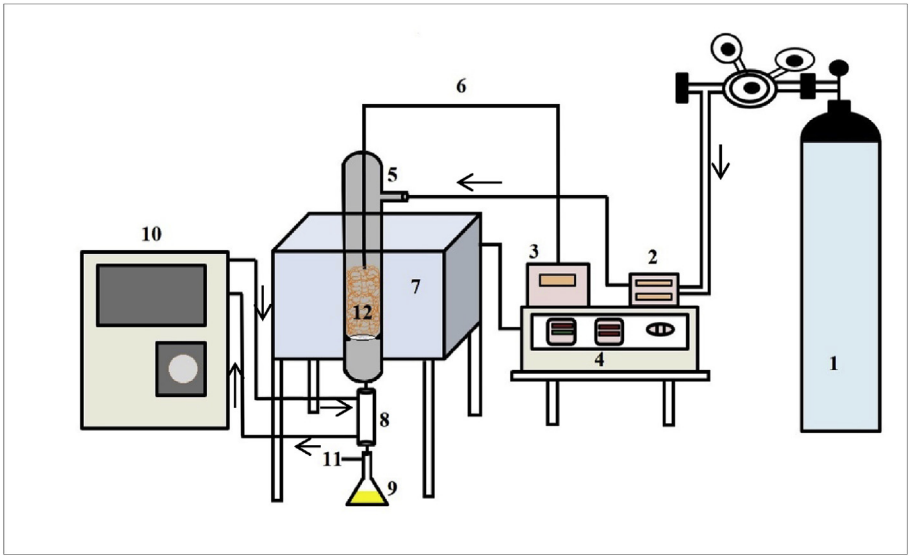

Fig. 1. Schematic diagram of experimental set-up: 1-nitrogen cylinder, 2-mass flow controller, 3-temperature measuring unit, 4- split tube furnace (NSW-104) controller, 5-long tube fixed bed reactor, 6-K-type thermocouple, 7- split tube furnace (NSW-104), 8-condenser, 9-oil collector, 10- chiller (Eyela CA-1112CE), 11-gas collector, 12-biomass with ceramic wool bed (Singh et al., 2019, 2020b, 2020a).

$$\text{Energy input} = \text{weight of raw biomass} \times \text{HHV of raw biomass} \quad (9)$$

$$\text{Energy output} = \text{weight of pyrolysis oil} \times \text{HHV of pyrolysis oil} \quad (10)$$

2.4. Analysis of pyrolysis oil, biochar and pyrolytic gases obtained at optimum condition of pyrolysis

The pyrolysis oil obtained from both the feedstocks at optimum conditions were subjected to estimation of physicochemical characteristics. The HHV of pyrolysis oil and biochar was enumerated using a bomb calorimeter (Model C-200, IKA, Germany). The Ramsbottom Carbon residue (RCR- IP 14/65) method was employed for the estimation of carbon residue of pyrolysis oil. ASTM D1298 protocol was employed to estimate the density of pyrolysis oil. The water content of pyrolysis oil was assessed by applying Karl Fischer titrator (ESICO, μP KARL FISCHER moisture titrator) following ASTM D1744 protocol. The viscosity of pyrolysis oil was measured using Brookfield digital viscometer (LVDV-II + Pro). The chemical characteristics, functional groups, and various classes of chemical compounds present in pyrolysis oil were examined by employing FTIR and GC-MS analyses, respectively. Fourier transform infrared spectroscopy (FTIR, Varian 1000, USA) was used to recognize the characteristic peaks associated with various chemical compounds associated with pyrolysis oil and biochar, while GC-MS (model-Shimadzu QP 2010 plus) was used to determine the relative amount of various class of chemical. Helium was used as a carrier gas with 1.21 mL/min flow rate. 1 μL of PO-RAW and PO-TB was injected (injector temperature of 260 °C) into the column (-RXi-5 Sil MS) having dimension of (30 m $\times$ 0.25 mm X 0.25 μm). The split ratio of column was 10:1. The initial temperature of GC oven was kept at 50 °C (5 min hold) and then heated to 250 °Cat a rate of 5 °C/min (again 5 min hold). Finally, the oven heated to 280 °Cat a rate of 10 °C/min for holding time of 5 min. The peaks obtained have been identified by using the National Institute of Standards and Technology library (NIST, USA). ^{13}C nuclear magnetic resonance spectrometry was used to analyze the various type of carbon, and their distribution in PO-RAW and PO-TB obtained at optimum condition of pyrolysis. The pyrolysis oil was dissolved in deuterated chloroform ($CDCl_3$), and NMR spectra were recorded by Bruker 500 MHz spectrometer (Magnetic system 500′54 ascend ULH) operating at 5 T with a 5 mm BBO BB-1H probe at room temperature with a relaxation delay of 2 s. The standard protocols ASTM E871 for moisture content, ASTM E1755 for ash content, and ASTM E872 for volatile matter were followed to execute proximate analysis of biochar from raw and TB. The fixed carbon of both biochars was obtained by difference. The CHNS analyzer instrument and software (EURO EA3000, EURO VECTOR, Italy) was used to investigate the elemental composition of both biochars. The elemental oxygen was obtained by difference considering insignificant sulfur content. The surface characteristics such as morphology and elements that exist on surface of biochar from pyrolysis of raw and TB were studied by Scanning Electron Microscopy (SEM) and Energy-Dispersive X-ray spectroscopy (EDX) (Model JEOL JSM5410, Japan). The pyrolytic gases were analyzed in gas chromatography (GC-TCD Centurion Scientific, model number-5800, New Delhi). Argon was used as carrier gas. The injector, column, and detector temperature were 80, 60, and 150 °C, respectively.

3. Results and discussion

3.1. Statistical analysis of developed model

Fig. 2 shows the actual and predicted values of response variable (pyrolysis oil yield), where 45° line represents the predicted yield, and the discrete data points represent experimental yield. It is perceived that both actual and predicted values of response are very close over a wide range of yield of pyrolysis oil; thus, it may be suggested that the developed model excellently represents pyrolysis data. Also, the correlation coefficient (R^2) value is 0.9758,

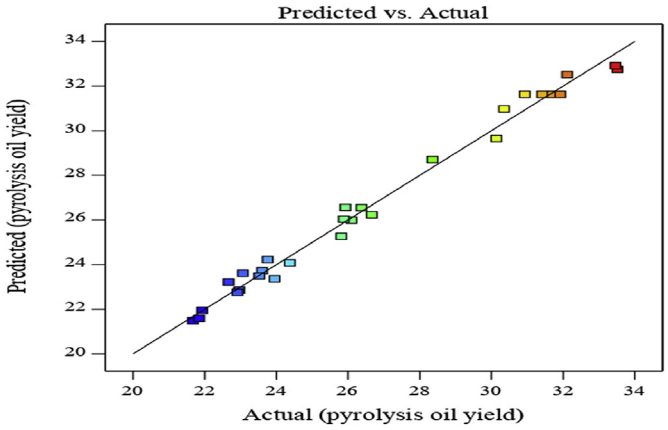

Fig. 2. Relationship between actual and predicted values of pyrolysis oil.

suggesting that developed relation between independent and dependent variables is highly reliable. The polynomial equation between response (pyrolysis oil yield) and variables (T (A), RT (B), HR (C), and SGF (D)) is given by Eq. (5).

$$Y_{\text{pyrolysis oil}}\ (\text{wt \%}) = 31.76 + 0.979A - 0.474B + 0.884C + 0.536AC + 0.599BC - 6.01A^2 - 1.90B^2 \quad (5a)$$

The statistical fitness of developed model has been investigated by ANOVA. The ANOVA is presented in Table 6. The statistical fitness of developed model is also confirmed by p-value, which is < 0.005, and higher F-value of 126.59. The model terms having a p-value $<$ 0.0500 are significant. In present developed model, A, B, C, AC, BC, A^2, B^2 are significant model terms. The discrepancy among predicted R^2 and adjusted R^2 should be < 0.2 for reasonable agreement between two coefficients. In this case, predicted R^2 and adjusted R^2 values were 0.9548 and 0.9681, respectively, showing a good agreement. Adequate precision signifies the signal to noise ratio, and its value should be > 4 for significant model. In the case of present developed model, the value of adequate precision was 30.403 showing that developed model can be used for design and scale-up.

3.2. Effect of process variables on yield of pyrolysis oil

3.2.1. Individual effect of process parameters

The pyrolysis of biomass was carried out by varying four independent parameters, namely, temperature, heating rate, retention time, and sweeping gas flow rate. The temperature during the pyrolysis supply the required heat for cleavage of bonds associated with biomass (Guedes et al., 2018). As a result, the pyrolysis oil yield increased with increase in temperature, however, after certain temperature, secondary cracking of volatiles dominates, which results in decrease in pyrolysis oil yield and increase in yield of pyrolytic gases (Guedes et al., 2018). The heating rate during the pyrolysis of biomass significantly affects the yield of pyrolysis oil. In the selected range of heating rate (15–40 °C/min), the yield of pyrolysis oil increased monotonously with heating rate. Thus, maximum yield of pyrolysis oil was obtained at 40 °C/min. The higher heating rate during pyrolysis favors the thermal cracking, fragmentation, and depolymerization reaction of biomass, which results in increase in yield of pyrolysis oil (Tripathi et al., 2016). The yield of pyrolysis oil decreased with increase in retention time during pyrolysis of biomass because higher retention time favors cross-linking and repolymerization reaction of biomass, which

Table 6
ANOVA of quadratic model for pyrolysis oil response and corresponding model terms.

Source	Sum of square	Degree of freedom	Mean of square	F-value	p-value	Remark
Pyrolysis oil yield						
Model	**450.70**	**7**	**64.39**	**126.59**	**< 0.0001**	Significant
A-Temp	17.28	1	17.28	33.97	<0.0001	Significant
B-RT	4.05	1	4.05	7.96	0.0100	Significant
C-HR	14.09	1	14.09	27.71	<0.0001	Significant
AC	4.61	1	4.61	9.07	0.0064	Significant
BC	5.76	1	5.76	11.32	0.0028	Significant
A^2	124.59	1	124.59	244.97	<0.0001	Significant
B^2	12.38	1	12.38	24.35	<0.0001	Significant
Residual	4.79	15	0.3191			
Lack of Fit	10.58	17	0.6223	5.10	0.0802	not significant
Pure Error	0.6097	5	0.1219			
Cor Total	461.89	29				
Std. Dev			0.7132	R-Squared		0.9758
Mean			27.01	Adjusted R-Squared		0.9681
C.V			2.64	Predicted R-Squared		0.9548
PRESS			27.24	Adequate Precision		30.407

supports the formation of biochar (Akhtar and Saidina Amin, 2012). The pyrolysis environment also affects the yield of pyrolysis oil. At lower sweeping gas flow rate, the interaction between vapor and solid causes exothermic reaction (Akhtar and Saidina Amin, 2012). As a result, biochar yield increased at lower sweeping gas flow rate. However, at very high sweeping gas flow rate, the condensable vapor might be drained out of the reactor, which may also decrease the yield of pyrolysis oil (Demiral and Şensöz, 2006). Meanwhile, it is important to mention that the effect of individual parameters is also governed by other parameters during pyrolysis process. The interaction of process variables is, therefore, of crucial importance for deciding the yield of pyrolysis oil.

3.2.2. Interaction effect of process parameters based on RSM on yield of pyrolysis oil

The effect of process variables (T, RT, HR, and SGF) on the pyrolysis oil yield was examined by 3D surface and contour plots using RSM exported from Design-Expert software. In 3D plots, the impact of two parameters was investigated at one time on pyrolysis oil yield. The remaining two parameters were kept constant because it is not possible to show the effect of more than two parameters simultaneously on 3D plots (Mohammed et al., 2017b). The significance of individual parameters, their interaction effect with each other, and square of parameters on pyrolysis oil yield was deduced using ANOVA.

Fig. 3 (a and b) represent the 3D surface and contour plot for pyrolysis oil yield where the combined influence of temperature and retention time at fixed heating rate (27.5 °C/min) and sweeping gas flow rate (60 mL/min) was examined. Results displayed that the pyrolysis oil yield increased to a maximum value, then started to decrease as the temperature and retention time continuously increased. An increase in temperature favors the formation of more volatiles; however, after specific temperature, due to secondary cracking reaction, volatiles might be converted into gaseous products such as H_2, CH_4, and CO (Guedes et al., 2018). While, increase in retention time favors the cross-linking and repolymerization reaction, which results in higher bio-char yield (Akhtar and Saidina Amin, 2012). From Table 6, it can be observed that temperature (A) is having F-value 33.97 and 244.97 for individual and square terms, respectively, and p-value less than 0.005 for both the terms. For retention time (B), the F-value for individual and square term is 7.96 and 24.35, respectively, and the p-value less was than 0.005 for both the terms. Thus, temperature (A) and retention time (B) individually and their squared terms (A^2, B^2) are significant for maximum yield of pyrolysis oil. However, interaction term (AB) related to temperature and retention time is not significant due to its p-value (0.2049) greater than 0.005. Similarly, the term (AD), which corresponds to the interaction between temperature and sweeping gas flow rate, is not significant because of higher p-value (0.1808). The p-value of all non-significant terms is not shown in ANOVA table since only significant terms have been considered and mentioned in ANOVA table.

The coupled impact of temperature and heating rate at fixed retention time and sweeping gas flow rate of 60 min and 60 mL/min, respectively, are displayed in Fig. 3 (c and d). The results inferred that pyrolysis oil yield increased with an increase in heating rate, and the maximum yield of pyrolysis oil was attained at the highest value of heating rate. In contrast to temperature, pyrolysis oil yield increased to a maximum value then started to decrease. The thermal cracking and fragmentation of biomass occur with increased heating rate during pyrolysis, which increases the pyrolysis oil yield (Tripathi et al., 2016). Also, heating rate during pyrolysis significantly affects the depolymerization reaction of biomass, which releases primary volatile components and added to the more liquid condensate (Dhyani and Bhaskar, 2018). Statistically, the individual term related to heating rate (C) and interaction term of heating rate with temperature (AC) is significant since both the terms have a lower p-value than 0.005 (Table 6). The F-values for temperature and heating rate are 33.97 and 27.71, respectively. Thus, the temperature influences pyrolysis more markedly than heating rate. However, the squared term related to heating rate (C^2) is not significant due to its higher p-value (0.5103).

Fig. 3 (e and f) display the coupled influence of temperature and sweeping gas flow rate at a constant heating rate (27.5 °C/min) and retention time (60 min). The result shows that the maximum pyrolysis oil yield was obtained at a minimum sweeping gas flow rate in the selected range (40–80 mL/min). At a higher gas flow rate, the vapor formed might be drained out from the condenser. As a result, pyrolysis oil yield decreases, and gaseous yield increases (Guedes et al., 2018). However, at a very low sweeping gas flow rate, retention time of vapor inside the reactor increases, which might result in a secondary cracking reaction of vapor (Tripathi et al., 2016). The statistical analysis confirmed that all the terms (individual, squared, and interaction with temperature) related to the sweeping gas flow rate are not significant for maximum yield of pyrolysis oil because of higher p-value (Table 6). The interaction effect of heating rate and retention time is shown in Fig. 3 (g and h), while, interaction effect of sweeping gas flow rate and retention time is shown in Fig. 3 (i and j). The flat nature of 3D plots indicates that coupled effect of these process variables on the yield of

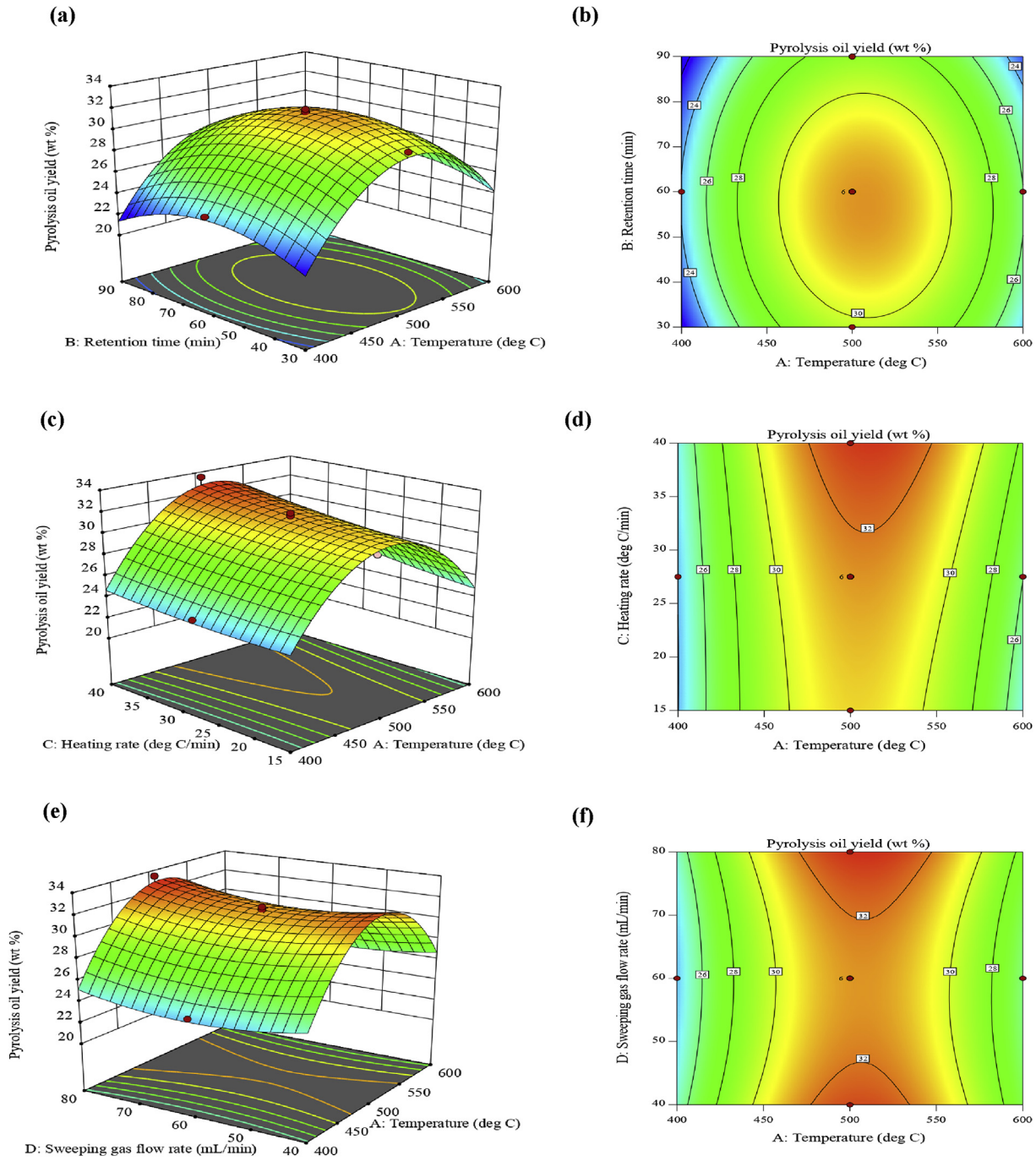

Fig. 3. Three dimensional response surface and contour plots of pyrolysis oil yield depicting the effect of (a) and (b) temperature and retention time, (c) and (d) temperature and heating rate, (e) and (f) temperature and sweeping gas flow rate, (g) and (h) retention time and heating rate, (i) and (j) retention time and sweeping gas flow rate, (k) and (l) heating rate and sweeping gas flow rate.

pyrolysis oil is minimal in the selected range of variables. Similar results were also obtained in case of effect of sweeping gas flow rate and heating rate on pyrolysis oil yield, as shown in Fig. 3 (k and l). Thus, based on the F-value obtained from ANOVA, temperature is the most significant parameter followed by heating rate, retention time, and sweeping gas flow rate, respectively, for maximum pyrolysis oil yield.

3.3. Validation of process parameters for yield of pyrolysis oil

The optimum condition for the experiment was attained by considering the independent process parameters in experimental range and dependent parameter (pyrolysis oil yield) to be the maximum (Table 7). Considering the above conditions, total hundred solutions were provided by the design expert statistical software. However, the solution having the highest desirability was taken into consideration. The optimum values of independent

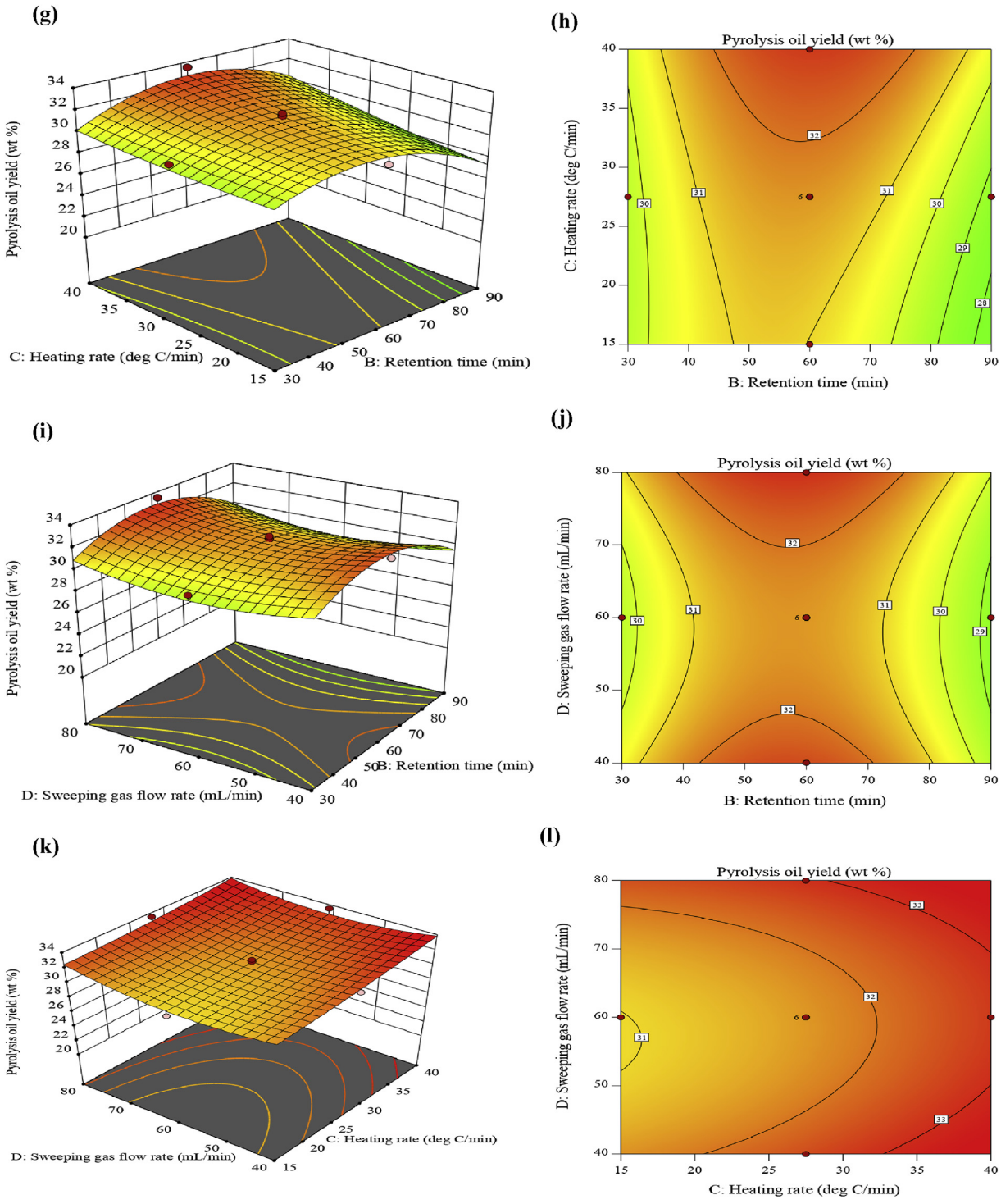

Fig. 3. (*continued*).

process variables for maximum pyrolysis oil yield (33.56 wt %) were found to be: T of 507.04 °C, RT of 58.25 min, HR of 38.00 °C/min, and SGF of 40.53 mL/min. This optimum condition obtained by design expert software was experimentally validated by performing the actual experiments at slightly different conditions (T of 507 °C, RT of 58 min, HR of 38 °C/min, and SGF of 40 mL/min) due to instrumental constraints of electric furnace and mass flow controller. The experimental and predicted values are given in Table 8. Based on the difference in experimental and predicted value of yield of

Table 7
Independent variables and response as constraints for optimization.

Parameters	Objective	Lower limit	Upper limit
Temperature (°C)	In range	400	600
Retention time (min)	In range	30	90
Heating rate (°C/min)	In range	15	40
Sweeping gas flow rate (mL/min)	In range	40	80
pyrolysis oil yield	Maximum	21.67	33.51

Table 8
Experimental and predicted values of pyrolysis oil yield at optimum condition.

Run	Temp (°C)	RT (min)	HR (°C/min)	SGF (mL/min)	Yield of pyrolysis oil from TB (wt %)		Error (%)
					Experimental	Predicted	
1	507	58	38	40	34.58	33.56	2.94
2	507	58	38	40	35.08	33.56	4.33
Average					34.83	33.56	3.64

At similar optimum condition the yield of pyrolysis oil for raw biomass was found to be 45.62 wt %

pyrolysis oil, the error was calculated and mentioned in Table 8. The experimental and predicted values for yield of pyrolysis oil were close enough (Error 3.64%) to certify the reliability of developed model. Further, at similar optimum conditions (T of 507 °C, RT of 58 min, HR of 38 °C/min, and SGF of 40 mL/min), pyrolysis of raw biomass was also performed to examine the differences in physicochemical properties of pyrolysis oil from raw and TB. During each pyrolysis experiment, 4 g of TB and raw biomass was used. The experiments were carried out in replicate, and average yield of pyrolysis oil was reported. The yield of pyrolysis oil at optimum condition was 34.83 wt % for pyrolysis of TB, while it was 45.62 wt % for pyrolysis of raw biomass.

3.4. Yield of pyrolysis oil, biochar and pyrolytic gases at optimum condition from pyrolysis of raw and TB

Table 9 represents the product yield obtained from pyrolysis of raw and TB at optimum condition of pyrolysis of TB for maximum pyrolysis oil yield. Results showed that yield of pyrolysis oil was 10.79 wt % lower, while, yield of pyrolytic gases and biochar was 3.05 and 7.74 wt %, respectively, was higher for TB as compared to raw biomass. These results were in accordance with the published literature (Chen et al., 2016b; Dai et al., 2019; Zheng et al., 2013). The yield of pyrolysis oil is lower due to lower volatile matter of TB and decomposition of lighter volatile compounds into CO_2, CO, H_2O, and acetic acid (Boateng and Mullen, 2013). Also, the higher ash content of TB (Singh et al., 2019) may catalyze the pyrolysis process to decrease the yield of pyrolysis oil by secondary cracking reaction (Yildiz et al., 2015). The solid biochar yield is higher (Boateng and Mullen, 2013; Singh et al., 2020b) because of higher cross-linking reaction and charring of TB during pyrolysis. The energy yield of pyrolysis oil was evaluated by employing Eq. (7). The energy yield of pyrolysis oil represents the amount of energy retained in the pyrolysis oil after pyrolysis (Singh et al., 2019). The energy yield of pyrolysis oil obtained from pyrolysis of raw and TB was found to be 58.42 and 53.15%, respectively. The lower value of energy yield for pyrolysis oil from TB was obtained because of lower pyrolysis oil yield (Chen et al., 2016a). The energy conversion efficiency for pyrolysis oil was evaluated by employing Eq. (8) and it was found to be 58.41 and 43.23% for pyrolysis oil from raw and TB, respectively. The lower energy conversion efficiency was noted for pyrolysis of TB due to lower yield of pyrolysis oil.

3.5. Characteristics of pyrolysis oil obtained at optimum condition of pyrolysis

3.5.1. Fourier transform infrared spectroscopy of pyrolysis oil

The FTIR analysis of PO-RAW and PO-TB obtained at optimum conditions are performed, and their spectra are depicted in Fig. 4. The FTIR spectra confirm the existence of various functional groups related to different classes of compounds. The stretching vibration of O—H between 3200 and 3400 confirms the presence of phenol, alcohol, water; while, vibration of C═O between 1680 and 1750 cm^{-1} corresponds to aldehyde and ketones (Gupta and Mondal, 2019). The vibration related to C—H stretching and deformation in the waveband of 2855—2926 and 1362-1462 cm-^{1}, respectively, corresponds to presence of alkane in pyrolysis oil (Mandal et al., 2018). The absorption band between 1420 and 1610 $cm^{-1}$and 690-900 cm^{-1} ascribes the presence of mono, polycyclic, and substituted aromatic compounds (Isa et al., 2011). Also, for PO-TB, the intensity of peaks are higher than PO-RAW, indicating the higher amount of aromatic compounds. The reduction of peaks intensity for PO-TB, between wave number 1100-1260 cm^{-1} attributed to reduction of oxygenated compounds related to alcohol and ether. The FTIR analysis provides a quick technique to identify the class of various chemical compounds (Isa et al., 2011), while gas chromatography-mass spectrometry analysis (GC-MS) can be employed for quantitative analysis of various chemical compounds present in pyrolysis oil.

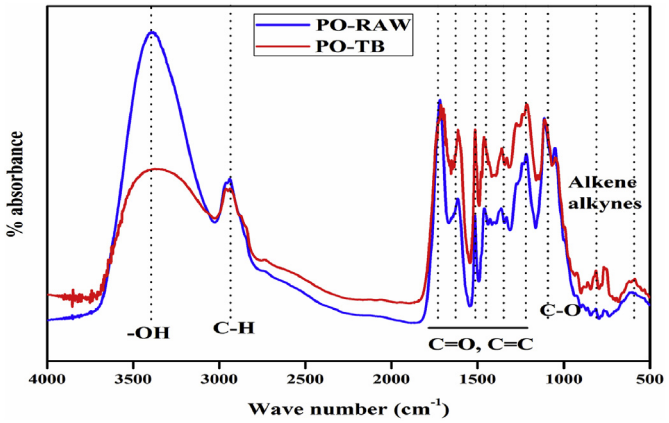

Fig. 4. FTIR spectra of pyrolysis oil from raw and TB at optimum condition.

3.5.2. Gas chromatography-mass spectrometry analysis pyrolysis oil

The GC-MS was performed to quantify the various class of chemical compounds exists in PO-RAW and PO-TB obtained at optimum condition of pyrolysis. The identified chemical compounds are listed in Table 10, while GC-MS spectra for PO-RAW and PO-TB are depicted in Figs. S1 (a) and (b) (Supplementary material). Results showed that PO-RAW and PO-TB contain various chemical compounds; however, in present study, they were grouped into eight major categories such as acid, aldehydes, ketones, alcohol, esters, phenol derivatives, furan derivatives and sugar derivatives based on their functional groups. It was noted that quantity of chemical compounds present in both pyrolysis oil varied significantly. Fig. 5 depicts the quantitative analysis of various classes of compounds based on the percentage area analyzed by GC-MS

Table 9
The average yield of pyrolysis oil, pyrolytic gases and biochar at optimum condition from pyrolysis of raw and TB.

Yield	Pyrolysis of raw biomass	Pyrolysis of TB
Pyrolysis oil (wt %)	45.62	34.83
Pyrolytic gas (wt %)	20.62	23.67
Biochar (wt %)	33.76	41.50

Table 10
Chemical composition of pyrolysis oil identified by GC-MS analysis at optimum condition of pyrolysis of raw and TB.

Compounds	Molecular formula	Relative content (peak area (%))	
		PO-TB	PO-RAW
Furan derivatives			
3-Furaldehyde	$C_5H_4O_2$	0.30	0.21
2-Furancarboxaldehyde	$C_5H_4O_2$	10.46	–
2-Furanmethanol	$C_5H_6O_2$	5.62	6.05
Furan, tetrahydro-2,5-dimethoxy-	$C_6H_{13}O_3$	1.04	0.62
2(3H)-Furanone, 5-Methyl-	$C_5H_6O_2$	3.52	5.02
2(5H)-Furanone,5-methyl-	$C_5H_6O_2$	–	0.27
2-Furancarboxaldehyde,-5-Methyl	$C_6H_6O_2$	–	6.45
2-Furanmethanol, Tetrahydro-	$C_5H_{10}O_2$	–	0.44
2-Dimethy(trimethylsilylmethyl)silyloxymethyltetrahydrofuran	$C_{16}H_{24}OSi$	–	0.08
Total		**20.94**	**19.14**
Phenol derivatives			
Phenol	C_6H_5OH	3.00	0.97
Phenol, 2-Methyl-	C_7H_8O	–	1.05
Phenol, 2-methoxy-	$C_7H_8O_2$	5.78	
Phenol, 4-methoxy-	$C_7H_8O_2$	–	8.72
Phenol, 2,6-dimethyl-	$C_8H_{10}O$	–	1.25
Creosol	$C_8H_{10}O_2$	3.84	6.05
Phenol, 4-ethyl-2-methoxy-	$C_9H_{12}O_2$	1.62	1.68
2-Methoxy-4-vinylphenol	$C_9H_{10}O_2$	3.79	1.14
Phenol, 2,6-dimethoxy-	$C_8H_{10}O_3$	9.46	9.11
Phenol, 3,4-dimethoxy-	$C_8H_{10}O_3$	–	0.75
3,5-Dimethoxy-4-hydroxytoluene	$C_9H_{12}O_3$	4.63	4.61
Phenol, 2-methoxy-4-(2-propenyl)-	$C_{10}H_{12}O_3$	3.67	0.64
Phenol, 2-methoxy-4-(1-propenyl)-,(E)-	$C_{10}H_{12}O_2$	0.91	–
Phenol, 2,6-dimethoxy-4-(2-propenyl)-	$C_{11}H_{14}O_3$	6.68	0.82
1-Hydroxy-2-methoxy-4-methylbenzene	$C_8H_{10}O_2$	0.37	–
Total		**43.75**	**36.79**
Acids			
dl-3-Methyl-dl-glutamic acid	$C_6H_{11}NO_4$	–	0.54
6-Heptenoic acid, methyl ester	$C_8H_{14}O_2$	–	0.21
Dimethylmalonic acid, dodecyl 3-ethylphenyl ester	$C_{28}H_{56}O_2$	–	0.41
3-Cyclopropenoic acid,-1-butyl, methyl ester	$C_9H_{14}O_2$	–	0.24
2,4-Hexadienedioic acid, 3,4-diethyl-, dimethyl ester, (E,Z)-	$C_8H_{10}O_4$	0.26	–
n-Hexadecanoic acid	$C_{16}H_{32}O_2$	0.60	0.54
Cyclopentanecarboxylic acid	$C_6H_{10}O_2$	0.15	–
Linoelaidic acid	$C_{18}H_{32}O_2$	–	1.90
9-Octadecenoic acid (z)-	$C_{18}H_{34}O_2$	–	0.15
Total		**1.01**	**3.99**
Alcohols			
1-Ethynyl-1-cycloheptanol	$C_8H_{12}O$	–	0.32
1-Penten-3-ol	$C_5H_{10}O$	0.80	0.65
1,2-Benzenediol, 3-methoxy-	$C_7H_8O_3$	0.66	0.28
1,2-Benzenediol, 3-methyl-	$C_7H_8O_2$	–	2.15
1,2,4-Benzenetriol	$C_6H_6O_3$	0.14	–
1-Octen-3-ol, acetate	$C_{10}H_{18}O_2$	0.82	–
3,4-Altrosan	$C_6H_{10}O_5$	0.37	–
trans-Sinapyl alcohol	$C_{11}H_{14}O_4$	0.14	–
Total		**2.93**	**3.40**
Aldehydes			
Benzaldehyde, 4-hydroxy-3-methoxy-	$C_8H_8O_3$	–	0.86
Benzaldehyde, 4-hydroxy-3,5-dimethoxy-	$C_9H_{10}O_4$	0.64	0.64
Coniferyl aldehyde	$C_{10}H_{10}O_3$	0.50	–
trans-Sinapaldehyde	$C_{11}H_{12}O_4$	0.55	–
Total		**1.69**	**1.5**
Ketones			
2-Pentanone, 4-hydroxy-4-methyl-	$C_6H_{12}O_2$	1.45	0.92
3-Penten-2-one, 3,4-dimethyl-	$C_7H_{12}O$	0.42	–
2-Cyclopenten-1-one, 2-methyl-	C_6H_8O	1.15	1.58
Alpha.,.beta.-crotonolactone	$C_4H_4O_2$	2.16	2.16
2-Methyl-3-hexanone	$C_7H_{14}O$	–	0.68
3-Methylcyclopentane-1,2-dione	$C_6H_8O_2$	2.86	3.93
5-Hydroxy-2-heptanone	$C_7H_{14}O_2$	0.30	0.46
Spiro[2.4]heptan-4-one	$C_7H_{10}O$	0.23	–
9-Oxabicyclo[6.1.0]non-6-en-2-one	$C_8H_{10}O_2$	0.14	–
3-Ethylcyclopent-2-en-1-one	$C_7H_{10}O$	–	0.25
4H-pyran-4-one, 3-hydroxy-2-methyl-	$C_6H_6O_3$	–	0.31
Ethanone, 1-(4-hydroxy-3-methoxyphenyl)-	$C_9H_{10}O_3$	0.34	0.25
Ethanone, 1-(4-hydroxy-3,5-dimethoxyphenyl)-	$C_{10}H_{12}O_4$	0.84	0.30
2-Cyclopenten-1-one, 3-ethyl-2-hydroxy-	$C_7H_{10}O_2$	0.54	–
6-Methoxycoumaran-7-ol-3-one	$C_9H_8O_4$	3.61	–
3′,5′-Dimethoxyacetophenone	$C_{10}H_{12}O_3$	–	0.41

(*continued on next page*)

Table 10 (*continued*)

Compounds	Molecular formula	Relative content (peak area (%))	
		PO-TB	PO-RAW
Total		**14.04**	**11.25**
Sugar derivatives			
1,4:3,6-Dianhydro-.alpha.-d-glucopyranose	$C_6H_8O_4$	0.30	1.47
2,3-Anhydro-d-mannosan	$C_6H_8O_4$	–	0.75
Beta.-D-Glucopyranose, 1,6-anhydro-	$C_6H_{10}O_5$	–	6.39
alpha.-D-Glucopyranose, 4-O-.beta.-D-galactopyranosyl	$C_{12}H_{22}O_{11}$	–	0.42
Total		**0.30**	**9.03**
Esters			
2-(Acetyloxy) Ethyl acetate	$C_7H_{12}O_5$	0.53	
Diethyl Phthalate	$C_{12}H_{14}O_4$	–	0.55
Di-n-octyl phthalate	$C_{24}H_{38}O_4$	0.35	0.31
1,2-Benzenedicarboxylic acid, diethyl ester	$C_{12}H_{14}O_4$	0.51	–
2,4-Hexadienedioic acid, 3,4-diethyl-, dimethyl ester, (E,Z)-	$C_8H_{10}O_4$	0.26 + 1.24	0.53
Total		**2.89**	**1.53**
Other compounds			
1H-Pyrazole, 3,5-dimethyl-	$C_5H_8N_2$	–	9.34
Bicyclo[2.2.2]octane, 1-fluoro-4-methyl-	$C_9H_{15}F$	–	0.27
Benzene, 1,2,3-trimethoxy-5-methyl-	$C_{10}H_{14}O_3$	3.18	1.91
Butane, 1-chloro-3,3-dimethyl-	$C_6H_{13}Cl$	–	0.32
1,4-Butanediamine, 2,3-dimethoxy-N,N,N′,N′-tetramethyl-, [S-(R*,R*)]-	$C_{10}H_{24}N_2O_2$	1.75	–
Total		**4.93**	**11.84**

analysis. The results showed that PO-TB contains lower acid, alcohol, and sugar derivatives than PO-RAW. Similar findings were also described by Xin et al. (2018), Ukaew et al. (2018). This decrease in oxygenated compounds will enhance the stability of pyrolysis oil. It will facilitate the use of pyrolysis oil in bio-refinery at lower cost (Ukaew et al., 2018). Meanwhile, PO-TB has higher percentage of furan derivatives, phenol derivatives, ketones, and esters than PO-RAW. The decomposition of acetoxy and methoxy groups from hemicellulose results in lower acid content (mainly carboxylic acid) in PO-TB and ketonization and rearrangement of carboxylic acid results in an increase in ketone content in PO-TB (Chen et al., 2017). Phenol derivative compounds were mainly formed due to decomposition of lignin present in biomass (Dai et al., 2019).

3.5.3. ^{13}C NMR analysis of pyrolysis oil

Apart from FTIR analysis, the functional groups and type of carbon present in the pyrolysis oil (PO-RAW and PO-TB) was also investigated by ^{13}C NMR analysis. The NMR spectra of PO-RAW and PO-TB are depicted in Fig. 6 (a) and (b). The NMR analysis has been considered as a powerful technique to classify the functional groups and type of carbon by dissolving the pyrolysis oil in a suitable solvent and quantify the functional groups by determining

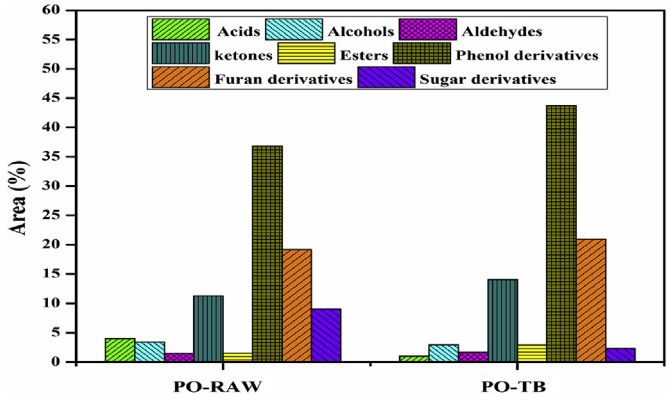

Fig. 5. The relative amount of different type of compound present in pyrolysis oil from raw and TB obtained at optimum condition.

the integral area of specific region of spectrum (Negahdar et al., 2016; Xu et al., 2019). The whole NMR spectrum was divided broadly into five chemical shift zones based on the previous work done by Negahdar et al. (2016), Ingram et al. (2008), and Joseph et al. (2010). The region from 0 to 54 ppm was assigned to alkyl carbon. Also, the alkyl carbon region was sub-divided into primary alkyl carbon (6–24 ppm) and secondary/tertiary alkyl carbon (24–34 ppm). The chemical shifts from 54 to 70 ppm, 70–103 ppm, 103–163 ppm, and 163–215 ppm were attributed to methoxyl/hydroxyl carbon, carbohydrate carbon, total aromatic carbon, and carbonyl carbon, respectively (Negahdar et al., 2016). Further, the aromatic carbon region was sub-divided into syringyl type carbon (110–112 ppm), guaiacyl type carbon (112–125 ppm). The results related to different types of carbon present in PO-RAW and PO-TB are presented in Fig. 7 (a) and (b), separately. The results showed that total aromatic carbon in PO-RAW and PO-TB was 24.65 and 34.58%, respectively. The increase in aromatic carbon in case of PO-TB may be due to higher lignin content in TB than the raw biomass (Negahdar et al., 2016). The alkyl carbon in PO-RAW and PO-TB was 36.57 and 28.21%, respectively. The total alkyl carbon in PO-TB decreased as compared to PO-RAW. However, primary alkyl carbon in PO-TB was higher than PO-RAW. This increases the utility of PO-TB as a fuel. The carbonyl carbon in PO-RAW and PO-TB was 10.24 and 15.5%, respectively. The increase in carbonyl carbon may be attributed to an increasing in ketones in case of PO-TB, as confirmed by GC-MS analysis. A slight decrease in methoxyl/hydroxy carbon was observed in case of PO-TB (13.16%) as compared to PO-RAW (15.5%). This may happen because of decrease in acid content in PO-TB. The carbohydrate carbon in PO-RAW and PO-TB was 13.04 and 8.55%, respectively. The ^{13}C NMR analysis of pyrolysis oil was consistent with the results of GC-MS analysis, as discussed in section 3.5.2.

3.5.4. Physicochemical characteristics of pyrolysis oil

The physicochemical characteristics of pyrolysis oil (PO-RAW and PO-TB) are mentioned in Table 11. The properties of PO-RAW and PO-TB were compared with standard specification protocol ASTM D7544-12 (ASTM-grade G and ASTM-grade D) (Mohammed et al., 2017b) and physical properties of mineral oils (Dhyani and Bhaskar, 2018). A Minor difference in appearances of PO-TB and PO-RAW was observed. PO-TB has an intense dark brownish color with no transparency, while PO-RAW has brownish color having

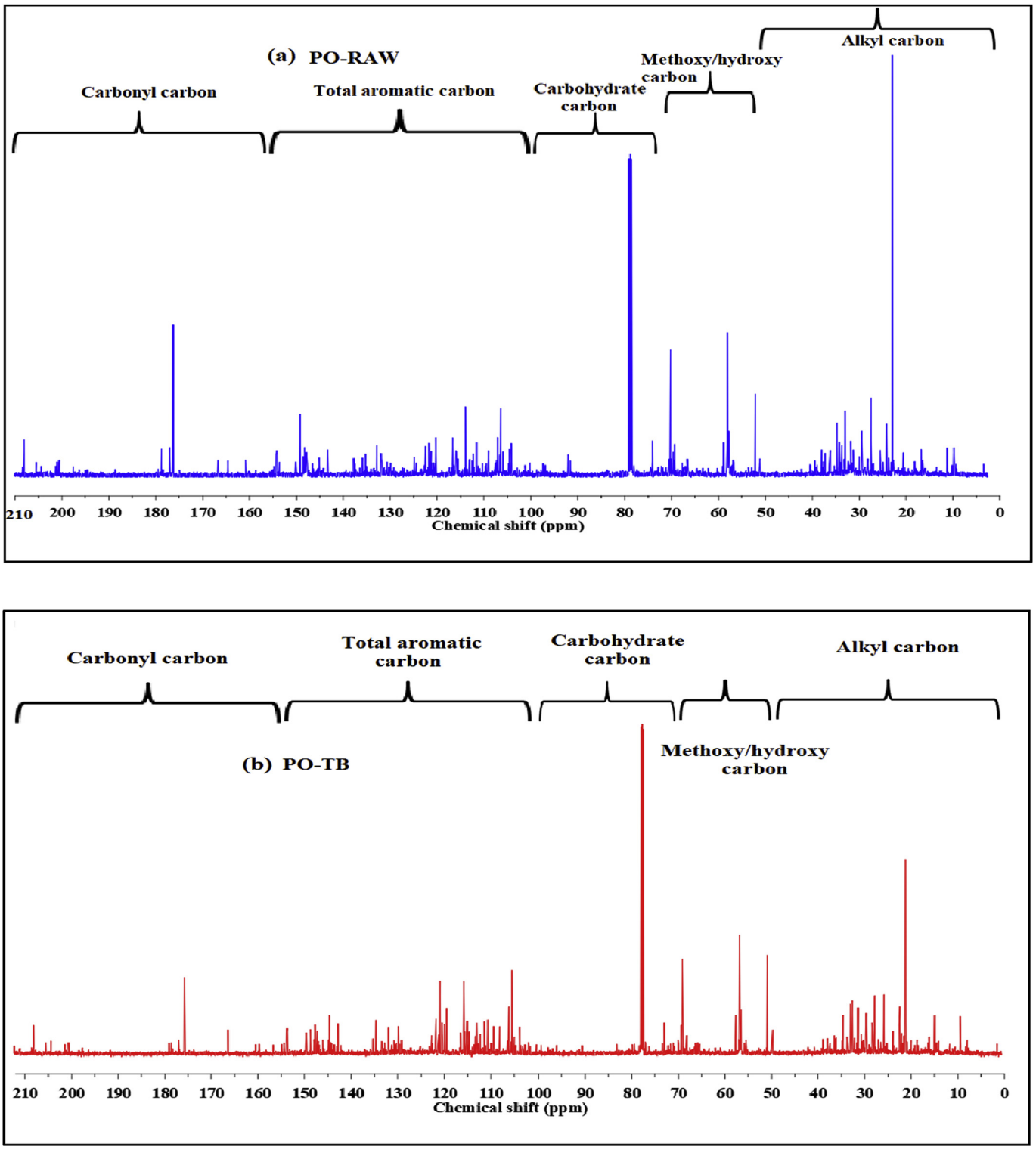

Fig. 6. ^{13}C NMR spectrum of pyrolysis oil obtained at optimum condition (a) PO-RAW, (b) PO-TB.

some transparency. The water content of PO-RAW and PO-TB was found to be 32 and 21 wt %, respectively. The water content in pyrolysis oil is associated with moisture content of native biomass and due to dehydration of pyrolysis products. Lower moisture content in TB is attributed to lower water content in PO-TB. The HHV of PO-RAW and PO-TB was 24.73 and 30.55 MJ/kg, respectively. The higher HHV of PO-TB is due to presence of various carbon-rich organic compounds (Mohammed et al., 2017b) and lower water content, which reduces the extra energy consumed in the evaporation of water present in pyrolysis oil. The density of PO-RAW and PO-TB was 1.098, 1.134 g/cm^3, respectively, while; viscosity was noted to 3.90 and 4.07 cSt, respectively. The lower water content for PO-TB may be attributed to increasing in density and viscosity. Both the pyrolysis oil (PO-RAW and PO-TB) show the

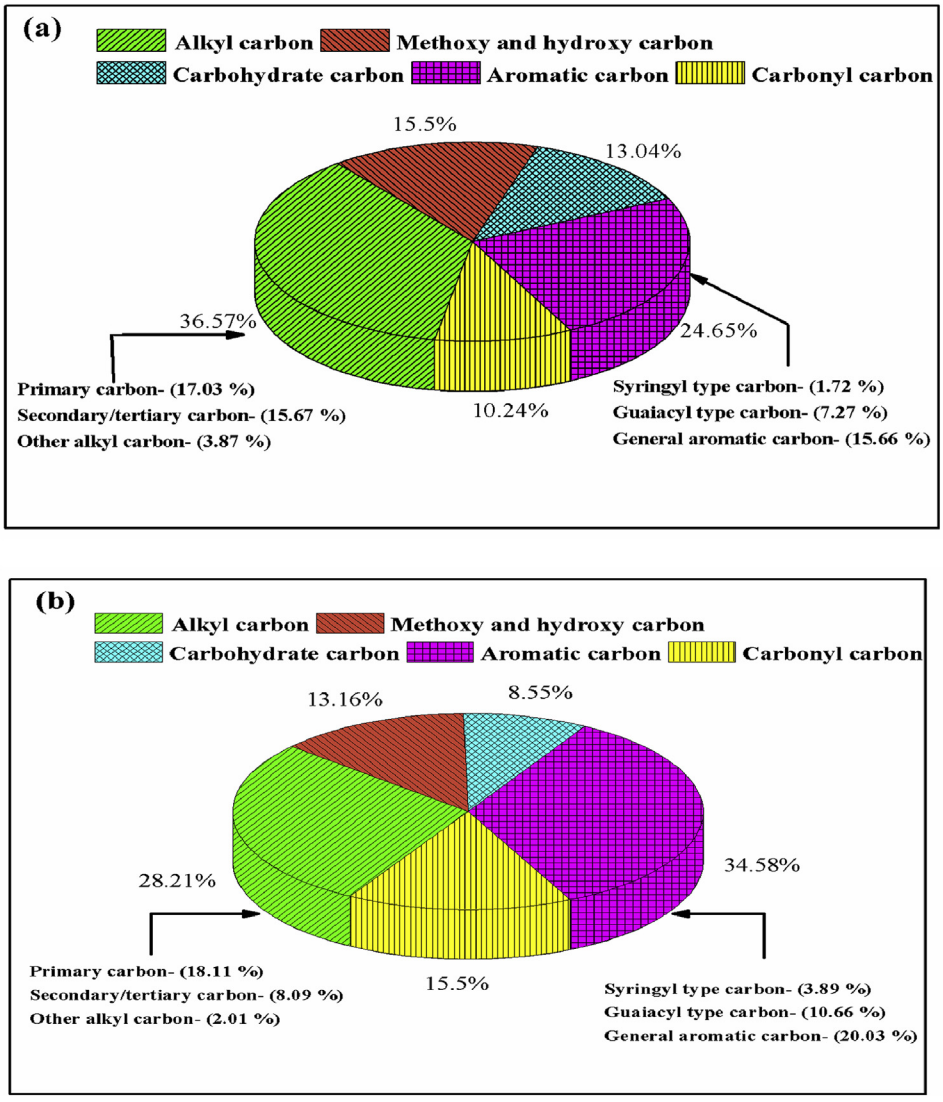

Fig. 7. The relative amount of different type of carbon present in pyrolysis oil obtained at optimum condition (a) PO-RAW, (b) PO-TB.

Table 11
Physicochemical properties of pyrolysis oil (PO-RAW and PO-TB) at optimum condition and comparison with ASTM grade oil and mineral oils (Dhyani and Bhaskar, 2018; Oasmaa et al., 2009).

Properties	PO-RAW	PO-TB	ASTM-Grade G	ASTM-Grade D	Heavy fuel oil	Light fuel oil
Appearance	Dark brown	Intense dark brown				
HHV (MJ/kg)	24.73	30.55	Minimum 15	Minimum 15	40.6	42.6
Density (g/cm^3)	1.098	1.134	1.1–1.3	1.1–1.3	0.99–0.995	0.845 (max)
Water content (wt. %)	32	21	Maximum 30	Maximum 30	~0	~0
pH	2.23	3.17	report	report	–	–
Carbon residue (wt. %)	2.78	3.21	–	–	–	–
Viscosity (cSt)	3.90	4.07	Maximum 125	Maximum 125	180–420	2.0–4.5
Ash content (wt. %)	0.03	0.01	Maximum 0.25	Maximum 0.15	0.08 (max)	0.01 (max)

acidic character having pH value of 2.23 and 3.17, respectively, because of acidic and phenolic compounds present in pyrolysis oil (Mohammed et al., 2017b). However, pH of PO-TB was 42.15% higher than the PO-RAW due lower of acidic components. Ramsbottom carbon residue of PO-RAW and PO-TB was found to be 2.78 and 3.21 wt %, respectively. It depicts the carbon deposition tendency of pyrolysis oil when it is used as a fuel. The ash content of PO-RAW and PO-TB was found to be 0.03 and 0.01 wt %, respectively. All physical parameters of PO-RAW and PO-TB were found in the range of ASTM-grade G and ASTM-grade D. However, PO-TB has improved properties than PO-RAW. The physical characteristics of both pyrolysis oil vary significantly as compared to mineral oils. This might be due to presence of water and oxygenated compounds present in pyrolysis oil. The higher water and oxygenated compounds attributed to lower heating value and high polarity of pyrolysis oil (Dhyani and Bhaskar, 2018).

3.5.5. Characteristics of biochar obtained at optimum condition from pyrolysis of raw and TB

3.5.5.1. Proximate and ultimate analyses of biochar. Table 12 represents the proximate and ultimate analyses of biochar from pyrolysis of raw (Biochar-raw) and TB (Biochar-torrefied). The moisture content and volatile matter decreased by 29.72 and 31.53%, while, fixed carbon and ash content increased by 4.58 and 29.58%, respectively, of Biochar-torrefied as compare to Biochar-raw. The difference in properties of both biochars was associated with the process through which they were obtained. Biochar-raw was obtained by pyrolysis of raw biomass, whereas, Biochar-torrefied was obtained by thermal treatment of raw biomass through torrefaction followed by pyrolysis. The intense devolatilization taking place in case of Biochar-torrefied results in lesser moisture content and volatile matter and relatively higher fixed carbon and ash content (Dai et al., 2019). Also, in case of Biochar-torrefied, the release of hydrogen and oxygen molecules was more prominent than the release of carbon as compared to the Biochar-raw. The HHV of Biochar-torrefied was 10.64% higher than the Biochar-raw. The higher HHV of Biochar-torrefied was attributed to higher carbon content than Biochar-raw. The results from proximate and ultimate analysis were similar to the finding of published literature (Chen et al., 2015a; Gogoi et al., 2017).

3.5.5.2. SEM-EDX analysis of biochar. Fig. 8 (a) and (b) depict the SEM-EDX analysis of Biochar-raw and Biochar-torrefied obtained at optimum condition of pyrolysis. Results showed that surface of both the biochars were heterogeneous, cracked, and having honeycomb-like pore structure (Dhanavath et al., 2019). Biochar-torrefied has wide pores as compare to Biochar-raw because of release of large amounts of volatile matter through intense devolatilization (Dhanavath et al., 2019; Gupta and Mondal, 2019). The pores present on the surface of both biochar may facilitate its potential application in adsorption process (Gupta and Mondal, 2019). EDX analysis confirmed that C, K, Ca, O, N existed on the surface of Biochar-raw, while, C, K, Ca, O, N, Mg existed on the surface of Biochar-torrefied. The presence of these macronutrients on the surface of biochar facilitates its utility in soil amendment (Mohammed et al., 2017b). Similar findings were also reported in published literature (Gupta and Mondal, 2019; Mohammed et al., 2017b).

3.5.5.3. FTIR analysis of biochar. The FTIR analysis of Biochar-raw and Biochar-torrefied was performed and their spectra are displayed in Fig. 9. The FTIR analysis provides a quick and efficient technique to identify the class of various chemical compounds. The FTIR spectra confirm the presence of various functional groups associated with biochar. For Biochar-raw, the peak at 3420.51 cm^{-1} corresponds to stretching vibration of O–H bonded groups such as phenol, alcohol, and water (Gupta and Mondal, 2019). The wavenumber 2925.68 cm^{-1} is ascribed to the stretching and deformation vibration of aliphatic C–H groups. The wavenumber 1688.47 cm^{-1} is assigned to C=O vibration of aldehyde and ketones and C=C aromatic vibrations. The wavenumber 1588.47 cm^{-1} corresponds to secondary amine groups. The wavenumber 1239.84 cm^{-1} is ascribed to deformative vibration of aromatic nitrogen to secondary amine groups. The wavenumber between 876.33 and 805.65 cm^{-1} and 757.12–686.51 cm^{-1} ascribe the presence of wagging vibration of C–H bond in aromatic ring and vibration of alkyl halide along with bending vibration of Si–O–Si bond, respectively. Similar results were obtained for Biochar-torrefied as well. However, the intensity of peaks for Biochar-torrefied was slightly lower than that of Biochar-raw. This might be due to torrefaction, as considerable rupture of –C-O, -O-H, etc. bonds take place, and there is formation of CO_2 and lighter non-condensable gases (Dai et al., 2019).

Table 12
Characteristics of biochar obtained at optimum condition from pyrolysis of raw and TB.

Analysis	Biochar-torrefied	Biochar-raw
Proximate analysis (wt %)		
Moisture content	0.78	1.11
Volatile matter	10.53	15.38
Ash content	8.76	6.97
Fixed carbon[a]	80.02	76.51
Ultimate analysis (wt %)		
C	86.17	81.38
H	1.01	1.98
N	3.34	2.48
S	BDL	BDL
O[a]	9.48	14.16
Higher heating value(MJ/kg)	30.55	27.61

[a] Calculated by difference, BDL; below detection limit.

3.5.6. Characteristics of pyrolytic gases obtained at optimum condition from pyrolysis of raw and TB

The composition of pyrolytic gases obtained from pyrolysis of raw and TB at optimum condition are displayed in Fig. 10. The pyrolytic gases from both the feedstock mainly consist of carbon dioxide (CO_2), carbon monoxide (CO), methane (CH_4) and hydrogen (H_2). Among all gases, the largest amount of CO_2 was present for both the feedstock followed by CO, CH_4, and H_2, respectively. However, significant difference was observed by comparing the composition of pyrolytic gases from raw and TB. The mass percentage of CO_2 decreased from 43.05 to 32.71%, while, mass percentage of CO, CH_4, and H_2 increased from 32.77 to 35.32, 20.64 to 25.26, 3.54–6.70%, respectively, for pyrolytic gases from TB as compared to raw biomass. CO_2 and CO formed during the pyrolysis as a result of decarboxylation and decorbonylation reactions, respectively (Wang et al., 2018). Thus, it can be concluded that decarboxylation reaction was more favorable for raw biomass, while, decarbonylation reaction was more favorable for TB. The decrease in CO_2 for TB pyrolysis was also attributed to degradation of hemicellulose during torrefaction (Konsomboon et al., 2019) The TB has higher lignin content as compared to raw biomass (Singh et al., 2020b). Cleavage of methoxyl group (-OCH_3) through demethoxylation reaction from benzene ring of lignin and presence of large number of alkyl branches in lignin mainly contributed to formation of H_2 and CH_4 (Shen et al., 2010). Small amount of CH_4 was also formed due to breakdown of hemicellulose and cellulose (Yang et al., 2007). The trend of formation of H_2 was in line with CH_4, revealing that generation of H_2 might be complemented by formation of CH_4 (Xin et al., 2013).

3.6. Mechanism of pyrolysis of TB

Torrefaction causes physical and chemical modifications in raw biomass due to which the pyrolysis pathway for TB differs from that of raw biomass because of changes in kinetic parameters, decrease in grinding energy, heat, and mass transfer rate, (Dai et al., 2019). In course of torrefaction, the methenyl groups associated with side chain of hemicellulose are broken, aldose groups detached from main chain of hemicellulose, and all the glycosidic bonds are ruptured; as a result, the hydroxyl bonds of hemicellulose are dehydrated (Dai et al., 2019). The fragmentation of cellulose occurred due to breaking of glycosidic and hydroxyl bonds associated with cellulose (Wang et al., 2017). In addition, slight modification of lignin takes place cleavage of β-O-4 ether bond of benzene ring associated with lignin (Mahadevan et al., 2016; Wen et al.,

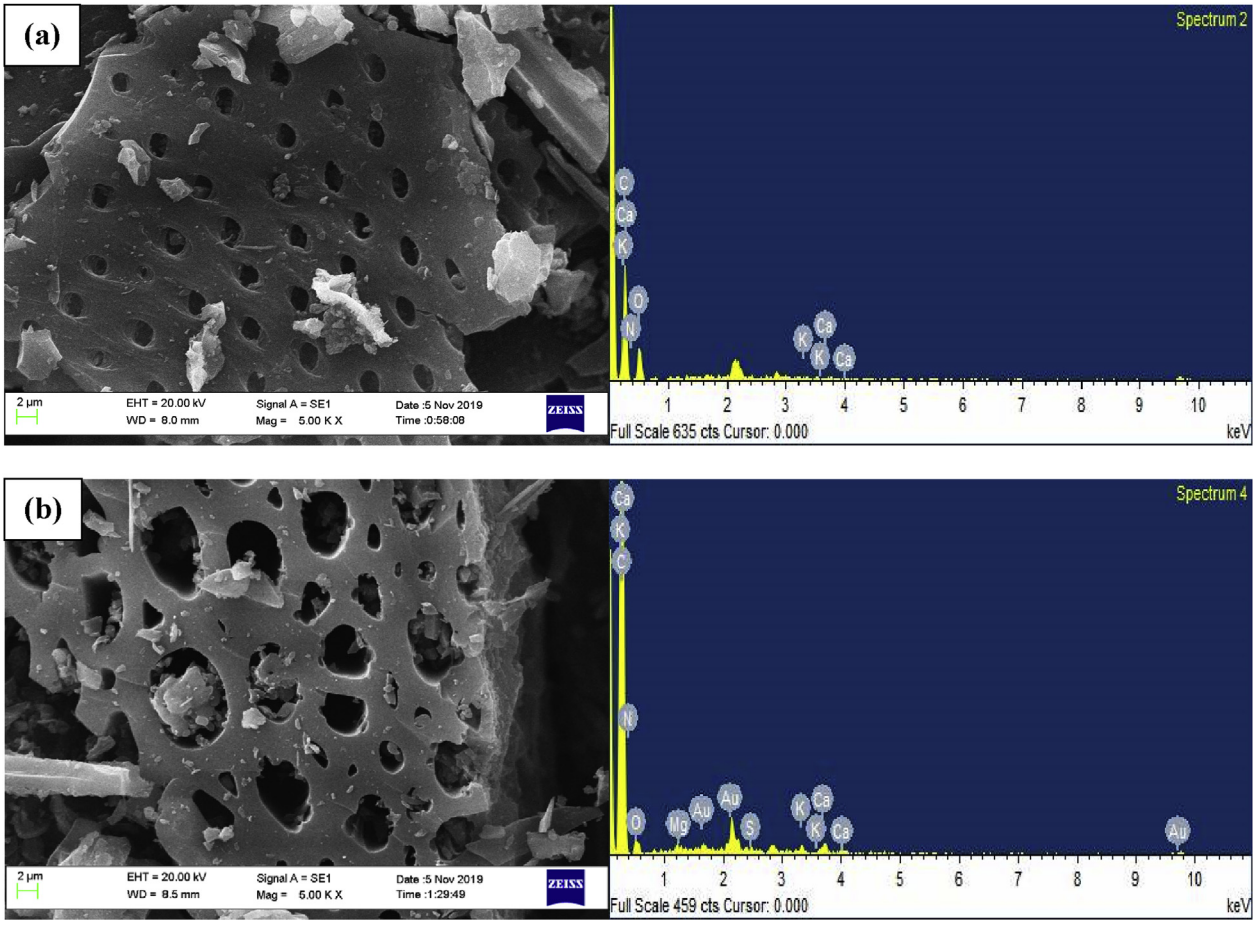

Fig. 8. SEM-EDX analysis of biochar at optimum condition **(a)** from pyrolysis of raw biomass **(b)** from pyrolysis of TB.

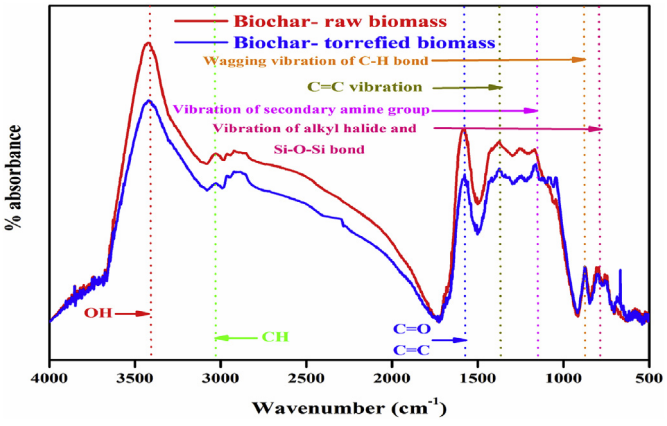

Fig. 9. FTIR spectra of biochar from raw and TB at optimum condition of pyrolysis.

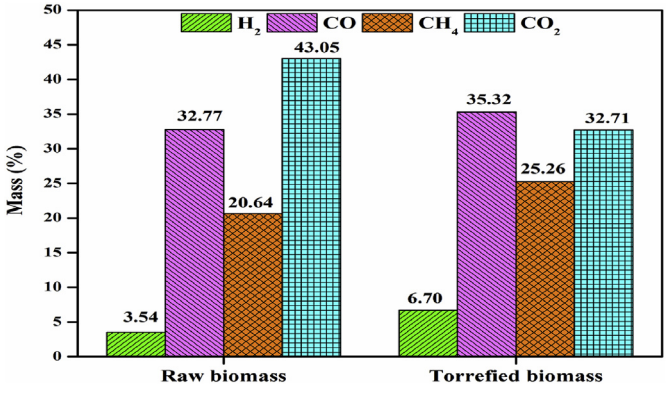

Fig. 10. Composition of pyrolytic gases from pyrolysis of raw and TB at optimum condition.

2014). The TB served better than the raw biomass since it has lower moisture and oxygen content along with a ruptured surface structure. TB has lower activation energy in comparison to raw biomass (Ren et al., 2013a), which is suggested by loose and porous structure (Singh et al., 2019). The yield of pyrolysis oil decreases when TB is pyrolysed (Boateng and Mullen, 2013; Chen et al., 2016b), as compared to pyrolysis of raw biomass; however, there is an enhancement in the characteristics of pyrolysis oil by means of lower water content, oxygenated compounds, and acid content. Also, the amount of total aromatic compounds increases (Chen et al., 2017). The yield of pyrolysis oil is lower due to lower volatile matter of TB and decomposition of lighter volatile compounds into CO_2, CO, H_2O, and acetic acid (Boateng and Mullen, 2013). Also, the higher ash content of TB (Singh et al., 2019) may catalyze the pyrolysis process to decrease the yield of pyrolysis oil by secondary cracking reaction (Yildiz et al., 2015). Also, the pyrolysis of TB favors the formation of CH_4 and H_2 as compared to CO_2 and CO (Ren et al., 2013b). The solid biochar yield is higher (Boateng and Mullen, 2013; Singh et al., 2020b) because of higher cross-linking reaction

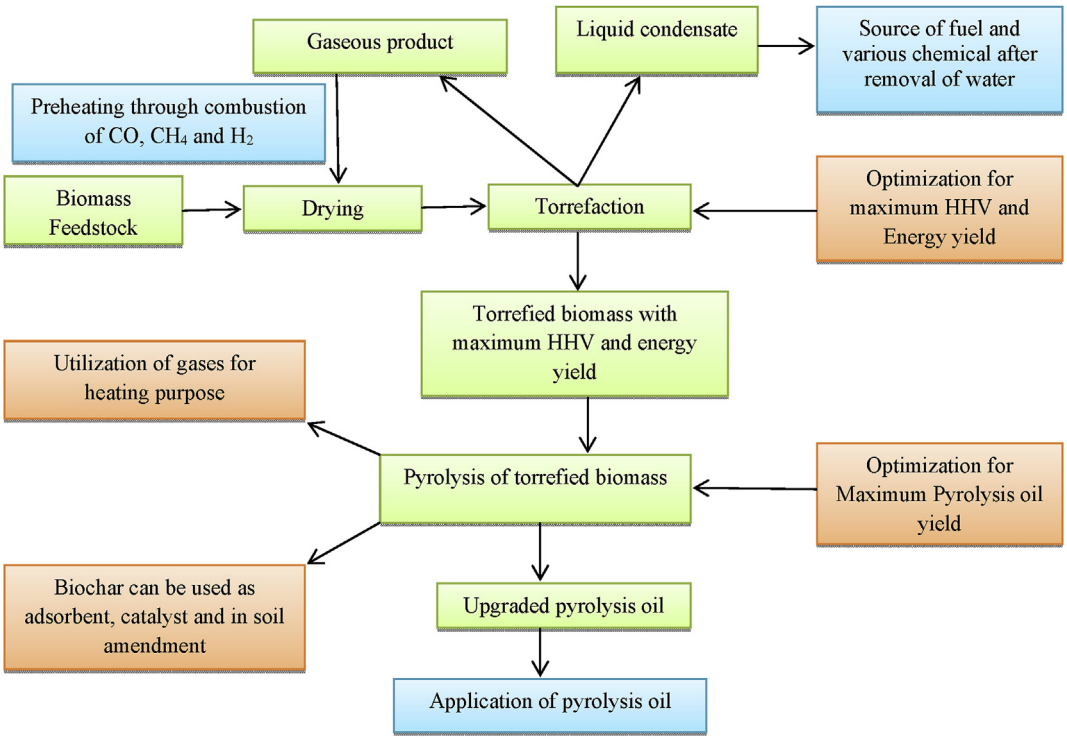

Fig. 11. Proposed way to increase the sustainability of integrated torrefaction-pyrolysis process.

and charring of TB during pyrolysis.

3.7. *Sustainability of integrated torrefaction-pyrolysis process and implication for cleaner production of pyrolysis oil*

Torrefaction was used as a pretreatment step. The desired product was high-quality solid biofuel. However, liquid condensate and gaseous products (CO_2 and CO in large quantity and CH_4 and H_2 in small quantity) are also produced during torrefaction (Chen et al., 2018; Ma et al., 2019). To increase the sustainability of integrated torrefaction-pyrolysis process, the gaseous products can be used in drying process through combustion of CO, CH_4, and H_2 or may be used to generate heat and electricity for integrated process (Dai et al., 2019). This will reduce the consumption of heat and electricity from external sources. The liquid condensate from torrefaction contains a number of C_1–C_4 oxygenated compounds (Doddapaneni et al., 2017; Liaw et al., 2015) and a large quantity of water (from 40 to 60 wt % depending on the condition of torrefaction) (Chen et al., 2015b; Ma et al., 2019). The liquid condensate may be used to digest CH_4 anaerobically (Doddapaneni et al., 2017; Liaw et al., 2015) or used as a fuel and source of various chemicals after removal of water. Besides, optimization of torrefaction process for high-grade solid biofuel in terms of maximum higher heating value and energy yield can further assist the overall economy, scale-up, and simulation of process by reducing the unnecessary experimental run (Singh et al., 2019). A general pathway for the sustainability of integrated process is shown in Fig. 11.

The pyrolysis oil obtained from pyrolysis of TB may have multiple applications, as shown in Fig. 12. As mentioned in section 3.5.1, the quality of pyrolysis oil obtained from TB is superior to pyrolysis oil obtained from raw biomass in terms of water content, pH value, HHV, etc. In section 3.5.3, it is mentioned that oxygen-containing compounds and total acidic compounds in pyrolysis oil from TB are lesser as compared to raw biomass. A pH close to 7 of pyrolysis oil is beneficial as it may reduce the corrosion in fuel system, other equipment, and piping systems during storage and transportation (Dai et al., 2019; Ma et al., 2019). Moreover, decreased water and oxygen-containing compounds may further facilitate upgrading of pyrolysis oil using suitable catalysts because water and oxygen-containing compounds are mainly responsible for coke formation and deactivation of sites on the surface of a catalysts (Dai et al., 2019). The application of pyrolysis oil has been reported by many authors. For instance, Kurji et al. (2016) used the blend of pyrolysis oil for turbine operation. Stamatov et at (Stamatov et al., 2006). used pyrolysis oil for heating in boilers, furnaces, and kiln and reported that during combustion brighter, shorter and wider flames were observed in case of pyrolysis oil as compared to diesel fuel. The biochar obtained from pyrolysis can be used in carbon sequestration, as an adsorbent in wastewater treatment, soil amendment, and as fuel (Dhyani and Bhaskar, 2018). The non-condensable gases produced may be used for external heating in other processes and recycling of gases into the pyrolytic reactor may enhance the heat integration as well as quality of pyrolysis oil (Mante et al., 2012). Besides, pyrolysis oil can be a good source of various chemical for industrial applications such as phenol and phenol derivatives such as methylphenols, methoxyphenols can be used in resin, food, paints and pharmaceutical industries (Stoikos, 1991), organic acids can be used for the synthesis of levoglucosan, de-icers, hydroxyacetaldehydes and other additives which can be used in fiber manufacturing, fertilizer and pharmaceutical industries (Bogner et al., 2008; Dhyani and Bhaskar, 2018). The aldehydes present in pyrolysis oil can be used as a browning agents for meat, fish, poultry, cheese, and sausages (Ingemarsson et al., 1998). In all these applications, the efficacy of pyrolysis oil from TB may be better as compared to pyrolysis oil obtained from raw biomass.

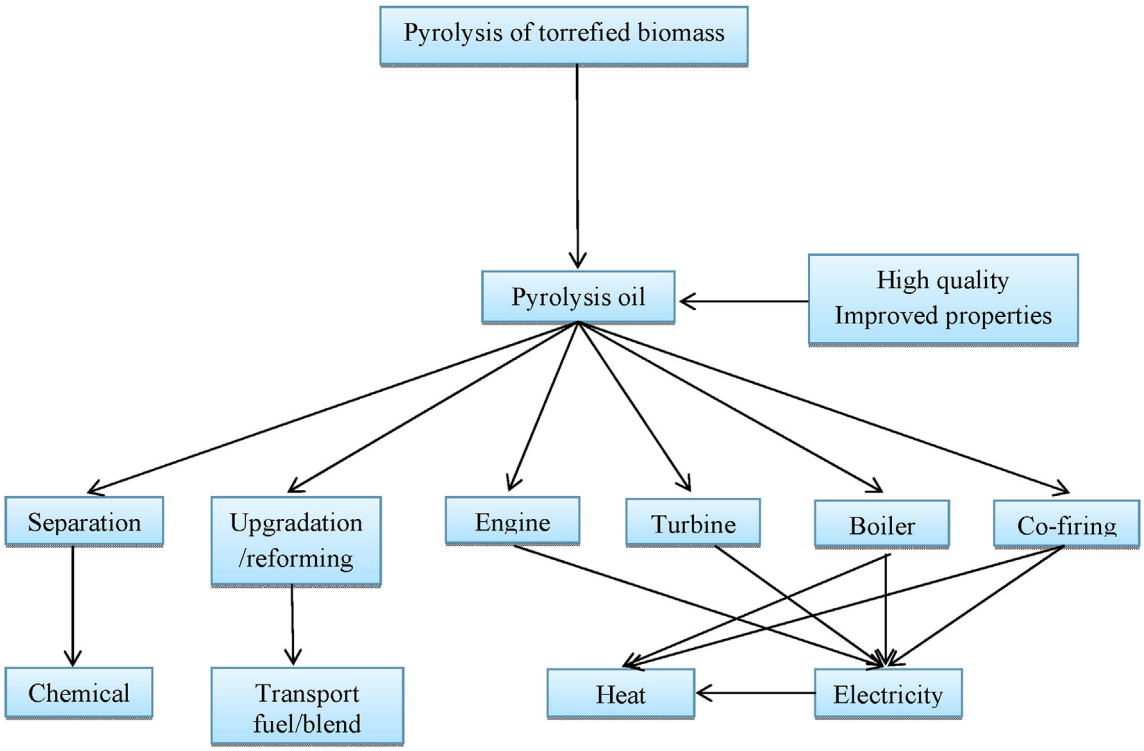

Fig. 12. Possible applications of pyrolysis oil from pyrolysis of TB (adapted from references (Bridgwater, 2012; Dhyani and Bhaskar, 2018)).

4. Conclusions and recommendations

Torrefaction improves many properties associated with raw biomass, while production of solid biofuels is the prime concern. Hence, pyrolysis of torrefied biomass was carried out to obtain high-quality pyrolysis oil. A response surface methodology coupled with central composite design was employed to optimize the process using temperature, retention time and heating rate, and sweeping gas flow rate as independent variables. The main objective was to maximize the yield of pyrolysis oil. To compare the physicochemical characteristics of pyrolysis oil, the raw biomass was also pyrolysed at the optimum condition, e.g., temperature = 507.04 °C, retention time = 58.25 min, heating rate = 38.00 °C/min, sweeping gas flow rate = 40.52 mL/min. It was observed that pyrolysis oil obtained from TB was superior in terms of improved HHV, pH, and chemical composition and lower water content, etc. Also, optimization of two processes (torrefaction and pyrolysis) may further facilitate design, scale-up, and simulation of process reactor system. The pyrolysis oil obtained from pyrolysis of torrefied biomass may be used effectively for direct heating in boilers and furnaces or as a blend in fossil-derived fuels. Also, many value-added chemicals such as phenol and furfural derivatives may be extracted from pyrolysis oil and may be used for manufacturing resin, polymer composites, etc., and as adhesives in cement manufacturing.

Furthermore, to increase the sustainability of integrated process, the energy supplied during the torrefaction process may be offset by utilizing the enthalpy of gaseous products from torrefaction in heat recovery, and liquid products may be utilized as fuel or source of chemical after removal of water. The application of suitable catalysts in pyrolysis of torrefied biomass may further increase the quality of pyrolysis oil and may mitigate the challenges of increased carbon residue and viscosity of pyrolysis oil obtained from torrefied biomass.

Thus, it may be concluded that combination of torrefaction with pyrolysis may increase the competitiveness of pyrolysis oil at a commercial scale due to its enhanced quality and improve overall sustainability in the biorefinery process, and also ensure waste minimization.

CRediT authorship contribution statement

Satyansh Singh: Data curation, Writing - original draft. **Jyoti Prasad Chakraborty:** Funding acquisition, Investigation, Project administration, Supervision. **Monoj Kumar Mondal:** Methodology, Writing - review & editing, Resources.

Declaration of competing interest

The authors declare that they have no known competing financial interests or personal relationships that could have appeared to influence the work reported in this paper.

Acknowledgement

The authors acknowledge the funding from the Science and Engineering Research Board (SERB), New Delhi, India, through fund no. SR/FTP/ETA-56/2012. Authors are thankful to Advance Instrument research facility, Jawaharlal Nehru University, New Delhi, for carrying out GC-MS analysis.

Appendix A. Supplementary data

Supplementary data to this article can be found online at https://doi.org/10.1016/j.jclepro.2020.122517.

References

Abas, F.Z., Ani, F.N., Zakaria, Z.A., 2018. Microwave-assisted production of optimized

pyrolysis liquid oil from oil palm fiber. J. Clean. Prod. 182, 404–413. https://doi.org/10.1016/j.jclepro.2018.02.052.
Akhtar, J., Saidina Amin, N., 2012. A review on operating parameters for optimum liquid oil yield in biomass pyrolysis. Renew. Sustain. Energy Rev. 16 (7), 5101–5109. https://doi.org/10.1016/j.rser.2012.05.033.
Boateng, A.A., Mullen, C.A., 2013. Fast pyrolysis of biomass thermally pretreated by torrefaction. J. Anal. Appl. Pyrolysis 100, 95–102. https://doi.org/10.1016/j.jaap.2012.12.002.
Bogner, J., Pipatti, R., Hashimoto, S., Diaz, C., Mareckova, K., Diaz, L., Kjeldsen, P., Monni, S., Faaij, A., Gao, Q., 2008. Mitigation of global greenhouse gas emissions from waste: conclusions and strategies from the intergovernmental panel on climate change (IPCC) fourth assessment report. Working group III (mitigation). Waste Manag. Res. 26 (1), 11–32. https://doi.org/10.1177/0734242X07088433.
Bridgwater, A.V., 2012. Review of fast pyrolysis of biomass and product upgrading. Biomass Bioenergy 38, 68–94. https://doi.org/10.1016/j.biombioe.2011.01.048.
Chen, D., Gao, A., Ma, Z., Fei, D., Chang, Y., Shen, C., 2018. In-depth study of rice husk torrefaction: characterization of solid, liquid and gaseous products, oxygen migration and energy yield. Bioresour. Technol. 253, 148–153. https://doi.org/10.1016/j.biortech.2018.01.009.
Chen, D., Li, Y., Cen, K., Luo, M., Li, H., Lu, B., 2016a. Pyrolysis polygeneration of poplar wood: effect of heating rate and pyrolysis temperature. Bioresour. Technol. 218, 780–788. https://doi.org/10.1016/j.biortech.2016.07.049.
Chen, D., Mei, J., Li, H., Li, Y., Lu, M., Ma, T., Ma, Z., 2017. Combined pretreatment with torrefaction and washing using torrefaction liquid products to yield upgraded biomass and pyrolysis products. Bioresour. Technol. 228, 62–68. https://doi.org/10.1016/j.biortech.2016.12.088.
Chen, D., Zheng, Z., Fu, K., Zeng, Z., Wang, J., Lu, M., 2015a. Torrefaction of biomass stalk and its effect on the yield and quality of pyrolysis products. Fuel 159, 27–32. https://doi.org/10.1016/j.fuel.2015.06.078.
Chen, W.-H., Liu, S.-H., Juang, T.-T., Tsai, C.-M., Zhuang, Y.-Q., 2015b. Characterization of solid and liquid products from bamboo torrefaction. Appl. Energy 160, 829–835. https://doi.org/10.1016/j.apenergy.2015.03.022.
Chen, Y., Cao, W., Atreya, A., 2016b. An experimental study to investigate the effect of torrefaction temperature and time on pyrolysis of centimeter-scale pine wood particles. Fuel Process. Technol. 153, 74–80. https://doi.org/10.1016/j.fuproc.2016.08.003.
Dai, L., Wang, Y., Liu, Y., Ruan, R., He, C., Yu, Z., Jiang, L., Zeng, Z., Tian, X., 2019. Integrated process of lignocellulosic biomass torrefaction and pyrolysis for upgrading bio-oil production: a state-of-the-art review. Renew. Sustain. Energy Rev. 107, 20–36. https://doi.org/10.1016/j.rser.2019.02.015.
Demiral, İ., Şensöz, S., 2006. Fixed-bed pyrolysis of hazelnut (Corylus avellana L.) bagasse: influence of pyrolysis parameters on product yields. Energy Sources Part A 28 (12), 1149–1158. https://doi.org/10.1080/009083190966126.
Dhanavath, K.N., Bankupalli, S., Sugali, C.S., Perupogu, V., V Nandury, S., Bhargava, S., Parthasarathy, R., 2019. Optimization of process parameters for slow pyrolysis of neem press seed cake for liquid and char production. J. Environ. Chem. Eng. 7 (1), 102905. https://doi.org/10.1016/j.jece.2019.102905.
Dhyani, V., Bhaskar, T., 2018. A comprehensive review on the pyrolysis of lignocellulosic biomass. Renew. Energy 129, 695–716. https://doi.org/10.1016/j.renene.2017.04.035.
Doddapaneni, T.R.K.C., Praveenkumar, R., Tolvanen, H., Palmroth, M.R., Konttinen, J., Rintala, J., 2017. Anaerobic batch conversion of pine wood torrefaction condensate. Bioresour. Technol. 225, 299–307. https://doi.org/10.1016/j.biortech.2016.11.073.
Dong, Q., Zhang, S., Ding, K., Zhu, S., Zhang, H., Liu, X., 2018. Pyrolysis behavior of raw/torrefied rice straw after different demineralization processes. Biomass Bioenergy 119, 229–236. https://doi.org/10.1016/j.biombioe.2018.09.032.
Gogoi, D., Bordoloi, N., Goswami, R., Narzari, R., Saikia, R., Sut, D., Gogoi, L., Kataki, R., 2017. Effect of torrefaction on yield and quality of pyrolytic products of arecanut husk: an agro-processing wastes. Bioresour. Technol. 242, 36–44. https://doi.org/10.1016/j.biortech.2017.03.169.
Guedes, R.E., Luna, A.S., Torres, A.R., 2018. Operating parameters for bio-oil production in biomass pyrolysis: a review. J. Anal. Appl. Pyrolysis 129, 134–149. https://doi.org/10.1016/j.jaap.2017.11.019.
Gupta, G.K., Mondal, M.K., 2019. Bio-energy generation from sagwan sawdust via pyrolysis: product distributions, characterizations and optimization using response surface methodology. Energy 170, 423–437. https://doi.org/10.1016/j.energy.2018.12.166.
Ingemarsson, Å., Nilsson, U., Nilsson, M., Pedersen, J.R., Olsson, J.O., 1998. Slow pyrolysis of spruce and pine samples studied with GC/MS and GC/FTIR/FID. Chemosphere 36 (14), 2879–2889. https://doi.org/10.1016/S0045-6535(97)10245-4.
Ingram, L., Mohan, D., Bricka, M., Steele, P., Strobel, D., Crocker, D., Mitchell, B., Mohammad, J., Cantrell, K., Pittman, C.U., 2008. Pyrolysis of wood and Bark in an Auger reactor: physical properties and chemical analysis of the produced bio-oils. Energy Fuels 22 (1), 614–625. https://doi.org/10.1021/ef700335k.
Isa, K.M., Daud, S., Hamidin, N., Ismail, K., Saad, S.A., Kasim, F.H., 2011. Thermogravimetric analysis and the optimisation of bio-oil yield from fixed-bed pyrolysis of rice husk using response surface methodology (RSM). Ind. Crop. Prod. 33 (2), 481–487. https://doi.org/10.1016/j.indcrop.2010.10.024.
Joseph, J., Baker, C., Mukkamala, S., Beis, S.H., Wheeler, M.C., DeSisto, W.J., Jensen, B.L., Frederick, B.G., 2010. Chemical shifts and lifetimes for nuclear magnetic resonance (NMR) analysis of biofuels. Energy Fuels 24 (9), 5153–5162. https://doi.org/10.1021/ef100504d.
Kadlimatti, H.M., Raj Mohan, B., Saidutta, M.B., 2019. Bio-oil from microwave assisted pyrolysis of food waste-optimization using response surface methodology. Biomass Bioenergy 123, 25–33. https://doi.org/10.1016/j.biombioe.2019.01.014.
Kılıç, M., Pütün, E., Pütün, A.E., 2014. Optimization of Euphorbia rigida fast pyrolysis conditions by using response surface methodology. J. Anal. Appl. Pyrolysis 110, 163–171. https://doi.org/10.1016/j.jaap.2014.08.018.
Konsomboon, S., Commandré, J.-M., Fukuda, S., 2019. Torrefaction of various biomass feedstocks and its impact on the reduction of tar produced during pyrolysis. Energy Fuel. 33 (4), 3257–3266. https://doi.org/10.1021/acs.energyfuels.8b04406.
Korshunov, A., Kichatov, B., Melnikova, K., Gubernov, V., Yakovenko, I., Kiverin, A., Golubkov, A., 2019. Pyrolysis characteristics of biomass torrefied in a quiescent mineral layer. Energy 187, 116015. https://doi.org/10.1016/j.energy.2019.116015.
Kurji, H., Valera-Medina, A., Runyon, J., Giles, A., Pugh, D., Marsh, R., Cerone, N., Zimbardi, F., Valerio, V., 2016. Combustion characteristics of biodiesel saturated with pyrolysis oil for power generation in gas turbines. Renew. Energy 99, 443–451. https://doi.org/10.1016/j.renene.2016.07.036.
Lazzari, E., Polidoro, A.d.S., Onorevoli, B., Schena, T., Silva, A.N., Scapin, E., Jacques, R.A., Caramão, E.B., 2019. Production of rice husk bio-oil and comprehensive characterization (qualitative and quantitative) by HPLC/PDA and GC × GC/qMS. Renew. Energy 135, 554–565. https://doi.org/10.1016/j.renene.2018.12.053.
Liaw, S.-S., Frear, C., Lei, W., Zhang, S., Garcia-Perez, M., 2015. Anaerobic digestion of C1–C4 light oxygenated organic compounds derived from the torrefaction of lignocellulosic materials. Fuel Process. Technol. 131, 150–158. https://doi.org/10.1016/j.fuproc.2014.11.012.
Ma, Z., Zhang, Y., Shen, Y., Wang, J., Yang, Y., Zhang, W., Wang, S., 2019. Oxygen migration characteristics during bamboo torrefaction process based on the properties of torrefied solid, gaseous, and liquid products. Biomass Bioenergy 128, 105300. https://doi.org/10.1016/j.biombioe.2019.105300.
Mahadevan, R., Adhikari, S., Shakya, R., Wang, K., Dayton, D.C., Li, M., Pu, Y., Ragauskas, A.J., 2016. Effect of torrefaction temperature on lignin macromolecule and product distribution from HZSM-5 catalytic pyrolysis. J. Anal. Appl. Pyrolysis 122, 95–105. https://doi.org/10.1016/j.jaap.2016.10.011.
Mandal, S., Bhattacharya, T.K., Verma, A.K., Haydary, J., 2018. Optimization of process parameters for bio-oil synthesis from pine needles (Pinus roxburghii) using response surface methodology. Chem. Pap. 72 (3), 603–616. https://doi.org/10.1007/s11696-017-0306-5.
Mante, O.D., Agblevor, F., Oyama, S., McClung, R., 2012. The influence of recycling non-condensable gases in the fractional catalytic pyrolysis of biomass. Bioresour. Technol. 111, 482–490. https://doi.org/10.1016/j.biortech.2012.02.015.
Meng, J., Park, J., Tilotta, D., Park, S., 2012. The effect of torrefaction on the chemistry of fast-pyrolysis bio-oil. Bioresour. Technol. 111, 439–446. https://doi.org/10.1016/j.biortech.2012.01.159.
Mohammed, I.Y., Abakr, Y.A., Xing Hui, J.N., Alaba, P.A., Morris, K.I., Ibrahim, M.D., 2017a. Recovery of clean energy precursors from Bambara groundnut waste via pyrolysis: kinetics, products distribution and optimisation using response surface methodology. J. Clean. Prod. 164, 1430–1445. https://doi.org/10.1016/j.jclepro.2017.07.068.
Mohammed, I.Y., Abakr, Y.A., Yusup, S., Kazi, F.K., 2017b. Valorization of Napier grass via intermediate pyrolysis: optimization using response surface methodology and pyrolysis products characterization. J. Clean. Prod. 142, 1848–1866. https://doi.org/10.1016/j.renene.2018.12.109.
Nazari, L., Yuan, Z., Ray, M.B., Xu, C.C., 2017. Co-conversion of waste activated sludge and sawdust through hydrothermal liquefaction: optimization of reaction parameters using response surface methodology. Appl. Energy 203, 1–10. https://doi.org/10.1016/j.apenergy.2017.06.009.
Negahdar, L., Gonzalez-Quiroga, A., Otyuskaya, D., Toraman, H.E., Liu, L., Jastrzebski, J.T.B.H., Van Geem, K.M., Marin, G.B., Thybaut, J.W., Weckhuysen, B.M., 2016. Characterization and comparison of fast pyrolysis bio-oils from Pinewood, Rapeseed cake, and wheat straw using 13C NMR and comprehensive GC × GC. ACS Sustain. Chem. Eng. 4 (9), 4974–4985. https://doi.org/10.1021/acssuschemeng.6b01329.
Oasmaa, A., Elliott, D.C., Müller, S., 2009. Quality control in fast pyrolysis bio-oil production and use. Environ. Prog. Sustain. Energy 28 (3), 404–409. https://doi.org/10.1002/ep.10382.
Ren, S., Lei, H., Wang, L., Bu, Q., Chen, S., Wu, J., 2013a. Thermal behaviour and kinetic study for woody biomass torrefaction and torrefied biomass pyrolysis by TGA. Biosyst. Eng. 116 (4), 420–426. https://doi.org/10.1016/j.biosystemseng.2013.10.003.
Ren, S., Lei, H., Wang, L., Bu, Q., Chen, S., Wu, J., Julson, J., Ruan, R., 2013b. The effects of torrefaction on compositions of bio-oil and syngas from biomass pyrolysis by microwave heating. Bioresour. Technol. 135, 659–664. https://doi.org/10.1016/j.biortech.2012.06.091.
Ro, D., Kim, Y.-M., Lee, I.-G., Jae, J., Jung, S.-C., Kim, S.C., Park, Y.-K., 2018. Bench scale catalytic fast pyrolysis of empty fruit bunches over low cost catalysts and HZSM-5 using a fixed bed reactor. J. Clean. Prod. 176, 298–303. https://doi.org/10.1016/j.jclepro.2017.12.075.
Saikia, R., Baruah, B., Kalita, D., Pant, K.K., Gogoi, N., Kataki, R., 2018. Pyrolysis and kinetic analyses of a perennial grass (Saccharum ravannae L.) from north-east India: optimization through response surface methodology and product characterization. Bioresour. Technol. 253, 304–314. https://doi.org/10.1016/j.biortech.2018.01.054.
Sakthivel, P., Subramanian, K.A., Mathai, R., 2020. Experimental study on unregulated emission characteristics of a two-wheeler with ethanol-gasoline blends

(E0 to E50). Fuel 262, 116504. https://doi.org/10.1016/j.fuel.2019.116504.
Sakthivel, R., Ramesh, K., Joseph John Marshal, S., Sadasivuni, K.K., 2019. Prediction of performance and emission characteristics of diesel engine fuelled with waste biomass pyrolysis oil using response surface methodology. Renew. Energy 136, 91–103. https://doi.org/10.1016/j.renene.2018.12.109.
Saratale, R.G., Saratale, G.D., Cho, S.-K., Ghodake, G., Kadam, A., Kumar, S., Mulla, S.I., Kim, D.-S., Jeon, B.-H., Chang, J.S., Shin, H.-S., 2019. Phyto-fabrication of silver nanoparticles by Acacia nilotica leaves: investigating their antineoplastic, free radical scavenging potential and application in H2O2 sensing. J. Taiwan Inst. Chem. Eng. 99, 239–249. https://doi.org/10.1016/j.jtice.2019.03.003.
Shen, D.K., Gu, S., Luo, K.H., Wang, S.R., Fang, M.X., 2010. The pyrolytic degradation of wood-derived lignin from pulping process. Bioresour. Technol. 101 (15), 6136–6146. https://doi.org/10.1016/j.biortech.2010.02.078.
Singh, S., Chakraborty, J.P., Mondal, M.K., 2019. Optimization of process parameters for torrefaction of Acacia nilotica using response surface methodology and characteristics of torrefied biomass as upgraded fuel. Energy 186, 115865. https://doi.org/10.1016/j.energy.2019.115865.
Singh, S., Chakraborty, J.P., Mondal, M.K., 2020a. Torrefaction of woody biomass (Acacia nilotica): Investigation of fuel and flow properties to study its suitability as a good quality solid fuel. Renew. Energy 153, 711–724. https://doi.org/10.1016/j.renene.2020.02.037.
Singh, S., Prasad Chakraborty, J., Kumar Mondal, M., 2020b. Intrinsic kinetics, thermodynamic parameters and reaction mechanism of non-isothermal degradation of torrefied Acacia nilotica using isoconversional methods. Fuel 259, 116263. https://doi.org/10.1016/j.fuel.2019.116263.
Stamatov, V., Honnery, D., Soria, J., 2006. Combustion properties of slow pyrolysis bio-oil produced from indigenous Australian species. Renew. Energy 31 (13), 2108–2121. https://doi.org/10.1016/j.renene.2005.10.004.
Stoikos, T., 1991. Upgrading of biomass pyrolysis liquids to high-value chemicals and fuel additives. In: Bridgwater, A.V., Grassi, G. (Eds.), Biomass Pyrolysis Liquids Upgrading and Utilization. Springer Netherlands, Dordrecht, pp. 227–241. https://doi.org/10.1007/978-94-011-3844-4_9.
Tripathi, M., Sahu, J.N., Ganesan, P., 2016. Effect of process parameters on production of biochar from biomass waste through pyrolysis: a review. Renew. Sustain. Energy Rev. 55, 467–481. https://doi.org/10.1016/j.rser.2015.10.122.
Ukaew, S., Schoenborn, J., Klemetsrud, B., Shonnard, D.R., 2018. Effects of torrefaction temperature and acid pretreatment on the yield and quality of fast pyrolysis bio-oil from rice straw. J. Anal. Appl. Pyrolysis 129, 112–122. https://doi.org/10.1016/j.jaap.2017.11.021.
Wang, S., Dai, G., Ru, B., Zhao, Y., Wang, X., Xiao, G., Luo, Z., 2017. Influence of torrefaction on the characteristics and pyrolysis behavior of cellulose. Energy 120, 864–871. https://doi.org/10.1016/j.energy.2016.11.135.
Wang, X., Wu, J., Chen, Y., Pattiya, A., Yang, H., Chen, H., 2018. Comparative study of wet and dry torrefaction of corn stalk and the effect on biomass pyrolysis polygeneration. Bioresour. Technol. 258, 88–97. https://doi.org/10.1016/j.biortech.2018.02.114.
Wen, J.-L., Sun, S.-L., Yuan, T.-Q., Xu, F., Sun, R.-C., 2014. Understanding the chemical and structural transformations of lignin macromolecule during torrefaction. Appl. Energy 121, 1–9. https://doi.org/10.1016/j.apenergy.2014.02.001.
Xin, S., Mi, T., Liu, X., Huang, F., 2018. Effect of torrefaction on the pyrolysis characteristics of high moisture herbaceous residues. Energy 152, 586–593. https://doi.org/10.1016/j.energy.2018.03.104.
Xin, S., Yang, H., Chen, Y., Wang, X., Chen, H., 2013. Assessment of pyrolysis polygeneration of biomass based on major components: product characterization and elucidation of degradation pathways. Fuel 113, 266–273. https://doi.org/10.1016/j.fuel.2013.05.061.
Xu, L., Cheng, J.-H., Liu, P., Wang, Q., Xu, Z.-X., Liu, Q., Shen, J.-Y., Wang, L.-J., 2019. Production of bio-fuel oil from pyrolysis of plant acidified oil. Renew. Energy 130, 910–919. https://doi.org/10.1016/j.renene.2018.07.012.
Yang, H., Yan, R., Chen, H., Lee, D.H., Zheng, C., 2007. Characteristics of hemicellulose, cellulose and lignin pyrolysis. Fuel 86 (12), 1781–1788. https://doi.org/10.1016/j.fuel.2006.12.013.
Yildiz, G., Ronsse, F., Venderbosch, R., van Duren, R., Kersten, S.R., Prins, W., 2015. Effect of biomass ash in catalytic fast pyrolysis of pine wood. Appl. Catal. B Environ. 168, 203–211. https://doi.org/10.1016/j.apcatb.2014.12.044.
Zhang, S., Chen, T., Xiong, Y., Dong, Q., 2017. Effects of wet torrefaction on the physicochemical properties and pyrolysis product properties of rice husk. Energy Convers. Manag. 141, 403–409. https://doi.org/10.1016/j.enconman.2016.10.002.
Zheng, A., Zhao, Z., Chang, S., Huang, Z., He, F., Li, H., 2012. Effect of torrefaction temperature on product distribution from two-staged pyrolysis of biomass. Energy Fuels 26 (5), 2968–2974. https://doi.org/10.1021/ef201872y.
Zheng, A., Zhao, Z., Huang, Z., Zhao, K., Wei, G., Wang, X., He, F., Li, H., 2014. Catalytic fast pyrolysis of biomass pretreated by torrefaction with varying severity. Energy Fuels 28 (9), 5804–5811. https://doi.org/10.1021/ef500892k.
Zheng, A.Q., Zhao, Z.L., Chang, S., Huang, Z., Wang, X.B., He, F., 2013. Effect of torrefaction on structure and fast pyrolysis behavior of corncobs. Bioresour. Technol. 128, 370. https://doi.org/10.1016/j.biortech.2012.10.067.
Zheng, Y., Tao, L., Yang, X., Huang, Y., Liu, C., Gu, J., Zheng, Z., 2017. Effect of the torrefaction temperature on the structural properties and pyrolysis behavior of biomass. BioResour 12 (2), 3425–3447. http://ncsu.edu/bioresources ISSN: 1930-2126.